UNIVERSIDAD AUTÓNOMA DE SAN LUÍS POTOSÍ

FACULTAD DE CIENCIAS QUÍMICAS, INGENIERÍA Y MEDICINA

PROGRAMAS MULTIDISCIPLINARIOS DE POSGRADO EN CIENCIAS AMBIENTALES

TESIS QUE PARA OBTENER EL GRADO DE

MAESTRÍA EN CIENCIAS AMBIENTALES.

ELIMINACIÓN DEL COLORANTE NEGRO REACTIVO 5 EN SOLUCIONES ACUOSAS MEDIANTE MATERIALES SINTÉTICOS A BASE DE CELULOSA, MAGNETITA Y POLIPIRROL.

PRESENTA:

L.Q CAMERINA JANETH GUZMÁN ALVAREZ

CO-DIRECTOR DE TESIS
DRA. PAOLA ELIZABETH DÍAZ FLORES
DR. VICTOR MANUEL OVANDO MEDINA

ASESOR.
DR. HUGO MAGDALENO RAMÍREZ TOBÍAS.

SAN LUIS POTOSI, S.L.P. ENERO 2019

CREDITOS INSTITUCIONALES.

PROYECTO REALIZADO EN:

LABORATORIO DE QUÍMICA AMBIENTAL DE LA FACULTAD DE AGRONOMÍA Y VETERINARIA DE LA UNIVERSIDAD AUTÓNOMA DE SAN LUIS POTOSÍ.

LABORATORIO DE OPERACIONES UNITARIAS DE LA COORDINACIÓN ACADÉMICA REGIÓN ALTIPLANO UNIVERSIDAD AUTÓNOMA DE SAN LUIS POTOSÍ.

CON FINANCIAMIENTO DE:

CONACYT PDCPN-2015-384, #25941

A TRAVES DEL PROYECTO DENOMINADO:

Remoción del colorante negro reactivo 5 a base de celulosa, magnetita y polipirrol.

LA MAESTRÍA EN CIENCIAS AMBIENTALES RECIBE APOYO ATRAVÉS DEL PROGRAMA NACIONAL DE POSGRADOS DE CALIDAD (PNPC)

DEDICATORIAS

A mi padre Dios por permitirme llegar hasta aquí y ser la mujer que soy, a mi adorado Pablo porque sin tu apoyo incondicional no podría haberlo logrado, a mi hermosa Madre, Silvia y Mario que cuidaron de mis hijos cuando no me era posible estar con ellos, a mis hijos Pablo y Camerina porque este esfuerzo fue pensando en ustedes.

Camerina.

AGRADECIMIENTOS.

Agradezco a aquellas personas que a través de las siguientes instituciones contribuyeron con este trabajo:

Universidad Autónoma de San Luis Potosí , Facultad de Agronomía y Veterinaria. Dra. Paola Elizabeth Díaz Flores, por su compromiso y dedicación a lo largo de la elaboración de este trabajo, por su asesoría, ideas, aportaciones y correcciones.

Universidad Autónoma de San Luis Potosí, Coordinación Académica Región Altiplano: Dr. Victor Manuel Ovando Medina, por su valioso asesoramiento, aportaciones y compromiso a lo largo de este trabajo y por permitirme el uso de los equipos del laboratorio. Dr. Miguel Corona y Dra. Elsa Cervantes por sus clases impartidas y aquellas personas que directa e indirectamente estuvieron presentes en esta etapa.

A todos, GRACIAS.

RESUMEN

En este trabajo se obtuvo un composito a partir de α-celulosa, la cual fue recubierta con nanopartículas de magnetita previamente sintetizadas y con polipirrol (PPy) semiconductor. Las nanopartículas de magnetita fueron sintetizadas por el método de coprecipitación a partir de las sales de $FeCl_2$ y $FeCl_3$ como precursores. El composito se obtuvo mediante la polimerización del pirrol en presencia de la mezcla de las nanopartículas de magnetita de α-celulosa. Las nanopartículas de magnetita y el composito, fueron caracterizados mediante espectroscopias de UV/Vis y FTIR, microscopia electrónica de barrido (SEM), espectrometría de dispersión de rayos X (EDS), difracción de rayos X (XRD), y análisis termogravimétrico (TGA). El análisis XRD mostró que las nanopartículas de magnetita presentan una estructura cúbica típica del Fe_4O_3. El análisis de SEM arrojó un tamaño promedio de partícula para la magnetita de 13 nm con morfología regular. Por otro lado, el composito se conforma de partículas esféricas de PPy recubriendo a la α-celulosa y a las nanopartículas de magnetita. El material sintetizado fue empleado en la remoción del colorante negro reactivo 5 (NR5) en soluciones acuosas a diferentes valores de cinética. La máxima capacidad de adsorción se observó a un pH de 3.0, con una capacidad de adsorción máxima de 62.31 mg de colorante/g de adsorbente, mientras que a pH de 7.0 fue de 21.67 mg/g. Los datos experimentales de las isotermas de adsorción para el colorante Negro Reactivo 5 fueron bien descritas mediante el modelo de Langmuir. El proceso de la cinética de adsorción del colorante NR5 en el composito fue descrito mediante un modelo de tres resistencias, permitiendo la estimación de la difusión, D_0, y del coeficiente de transferencia externa, k_1. Para los experimentos de adsorción a pH 3.0, la D_0 fue de 4.37×10^{-11} m^2/s mientras que k_1 fue de 7.30×10^{-7} L/mg·s.

Palabras *clave: nanopartículas de magnetita; polipirrol; colorante; adsorción; composito.*

ABSTRACT.

A composite was obtained from α-cellulose coated with magnetite nanoparticles and conducting polypyrrole (PPy). The magnetite nanoparticles were synthesized by the co-precipitation method from $FeCl_2$ and $FeCl_3$ salts. The composite was obtained by pyrrole polymerization in the presence of a mixture of α-cellulose and magnetite nanoparticles. The magnetite nanoparticles and composite were characterized by FTIR and UV/Vis-NIR spectroscopies, scanning electron microscopy (SEM), energy dispersive spectroscopy (EDS), X-ray diffraction (XRD), and thermogravimetric analyses (TGA). XRD analysis demonstrated that magnetite nanoparticles with the typical cubic structures of Fe_3O_4 were obtained. SEM analysis showed that magnetite nanoparticles had irregular morphology with average size of 13 nm, whereas the composite consisted of spherical nanoparticles of PPy coating α-cellulose fibers and magnetite nanoparticles. Batch aqueous adsorption experiments of the reactive black 5 (RB5) dye onto the synthesized material were conducted. The results showed that for the adsorption experiments set to initial pH of 3.0; the maximum adsorption capacity was 62.31 mg of dye/g of composite, while a value of 21.67 mg of dye/g of composite was obtained when the initial solution pH was set to 7.0. Adsorption isotherms data for the RB5 dye were well described by the Langmuir model. The transient adsorption process of the RB5 dye onto the composite was described by a general three-resistance model; allowing the estimation of the effective diffusivity, D_0, and the adsorption rate coefficient, k_1. For the adsorption experiments with an initial pH value set to 3.0, D_0 was estimated as 4.37×10^{-11} m^2/s while k_1 was 7.30×10^{-7} L/mg·s.

Keywords: *magnetite nanoparticles; polypyrrole; dye; adsorption; composite.*

1. Introducción.

De acuerdo con el Informe sobre el desarrollo Mundial del Agua de la ONU, el uso del agua y la generación de aguas residuales debido a actividades antropogénicas ha ido incrementado su demanda y por lo tanto la generación de contaminantes. Alrededor de un 80% del agua residual generada en todo el mundo y el 95% en algunos países subdesarrollados son vertidos al medio ambiente sin ningún tipo de tratamiento. Esta agua generalmente es descargada en los cuerpos acuosos, infiltrándose en los mantos acuíferos, afectando la calidad de los suministros de agua dulce (ONU, 2017).

La industria textil y del cuero, demanda grandes cantidades de agua y sus efluentes son altamente contaminantes. Por eso el tratamiento del agua residual se ha convertido en un reto global para los científicos y los gobiernos, y al mismo tiempo un mercado atractivo de desarrollo en tecnologías de purificación del agua.

Por ejemplo, en el mercado de las membranas de ósmosis inversa, está actualmente proyectado hacer crecer su mercado en un 10% anual, durante los próximos tres años. En el caso de resinas de intercambio iónico, se estima un crecimiento en promedio del 4% anual (WWI, 2017).

En el desarrollo de nuevos materiales adsorbentes; es importante considerar varios factores como la disponibilidad de materias primas, fácil síntesis, bajo costo, regeneración, y recuperación física del material adsorbente. En este sentido, se han estudiado y preparado diferentes materiales como adsorbentes naturales, entre ellos se encuentran el uso de fibras de coco de desecho (Hamed et al. 2008), carbón activado de cáscara de coco (Tan et al, 2008), el gusano de seda (Noroozi et al, 2007), zeolitas (Hor Et al, 2016; Saptura et al, 2016; Humelnicu et al 2017) y las plantas (Aziam et al, 2016). Sin embargo, se ha observado que los compositos de dos o más adsorbentes naturales o adsorbentes naturales con polímeros sintéticos pueden mejorar la eficiencia en la remoción de colorantes en el agua residual. (Perez-Escobedo et al, 2016) ha reportado el uso de quitosan/zeolita y

alga/quitosan para la adsorción de flúor en soluciones acuosas, observandose que a pH de 5 el composito de quitosan/zeolita tiene un incremento en la capacidad de adsorción de flúor que cuándo se adsorbe en alga/quitosan a un pH de 7. Habiba et al, (2017) prepararon una mezcla de zeolita/alcohol polivinílico para la remoción de naranja de metilo y rojo congo a través de coagulación y procesos de adsorción, observando buena capacidad en la remoción de contaminantes.

El interés en la preparación de compositos con adsorbentes naturales y polímeros sintéticos ha ido en aumento debido a los bajos costos siempre y cuando puedan ser originados de desperdicios (por ejemplo, los materiales lignocelulósicos). Además, los adsorbentes naturales pueden ser fácilmente combinados con pequeñas cantidades de polímeros sintéticos; a los cuales les confiere propiedades de mejor adsorción. Particularmente, los polímeros conductores como el PPy y la polianilina los cuales son de gran interés debido a su buena estabilidad en el ambiente, síntesis sencilla, y conductividad eléctrica alta (Wang et al, 2005). En este sentido, se ha reportado la síntesis del composito de sorgo/PPy mediante oxidación química de pirrol. Este composito se empleó en la remoción del colorante azul de metileno en soluciones acuosas; obteniendo una máxima capacidad de adsorción de 143.5 mg/g (66.4% más que con fibras de sorgo solas) (Ovando-Medina et al, 2014). Un trabajo similar fue reportado por (Ansari et al, 2010) quien preparó un composito de aserrín de árbol de nogal y polianilina; para la adsorción del colorante azul de metileno en soluciones acuosas a temperatura ambiente y pH 9. De acuerdo con la isoterma de Langmuir, la máxima capacidad de adsorción fue 8.3mg/g. Sin embargo, al usar PPy en lugar de polianilina la máxima capacidad de adsorción aumentó a 34.3mg/g (Ansari et al, 2010). Recientemente se reportó un composito de celulosa/PPy en la remoción del colorante rojo reactivo 120 en soluciones acuosas, observando una máxima capacidad de adsorción de 96.1 mg/g a pH ácido (Ovando-Medina. 2015).

Así, la combinación de adsorbentes naturales y los polímeros semiconductores incrementan la capacidad de adsorción de algunos compuestos. Sin embargo, desde un

punto de vista práctico, la recuperación del adsorbente después de la adsorción del colorante es muy importante ya que el adsorbente saturado tiene que ser dispuesto o regenerado para su reutilización. Una opción para superar este problema de recuperación es la síntesis o preparación de materiales con propiedades magnéticas que puedan ser separados usando campos magnéticos externos. Actualmente, los investigadores se están enfocando en la síntesis de nanopartículas magnéticas basadas en hierro debido a sus propiedades; lo cual permite su aplicación en los campos de la química y la ingeniería. En contraparte con su tamaño voluminoso; las nanopartículas de Fe_3O_4 poseen mayor número de propiedades físicas y químicas debido a su efecto mesoscópico, cuántico, de superficie, de carácter superparamagnetico, y no tóxico (Bagheri et al, 2017). Algunos resultados de estudios en compositos de magnetita/PPy fueron reportados por Bai et al, (2015), quien preparó un nanocomposito de grafeno, polipirrol y magnetita (Fe_3O_4/PPy/RGO) y estudió su capacidad de remoción del colorante azul de metileno en solución acuosa. Estos investigadores observaron, de acuerdo a su isoterma de Langmuir, una máxima capacidad de adsorción de azul de metileno de 270.3mg/g. En otro trabajo, Ayad et al, (2014) reportó la síntesis del composito quitosán/PPy/magnetita para la remoción del colorante ácido verde 25; observando una mayor capacidad de adsorción que con quitosán y PPy por si solos. Las propiedades magnéticas del composito permitieron su recuperación al final del proceso de adsorción. Asgharinezhad et al. (2015) usaron un composito de nanotubos de carbono multicapa/nanopartículas de magnetita/PPy en la co-extración de contaminantes ácidos, básicos, y anfotéricos (polares y no polares).

El propósito del presente trabajo fue la síntesis y caracterización de un composito de celulosa recubierta de nanopartículas de magnetita y PPy semiconductor. Este composito se empleó en la remoción del colorante aniónico Negro Reactivo 5 (NR5) (Tetrasodio -4-amino-hidroxi-3,6 (Bis(4-(2-(Sulfonatooxi) Etilsulfonil) Fenil) Azo) – Naftaleno- 2,7-disulfonato) es un colorante di-azosulfónico, compuesto por un complejo auxocromo y cromóforo, constituido por el grupo azo y anillos aromáticos unidos a este, cuya estructura

se muestra en la Fig. 1, presente en soluciones acuosas. El modelo matemático de tres resistencias se usó para describir el mecanismo de adsorción de los colorantes en la superficie del composito sintetizado.

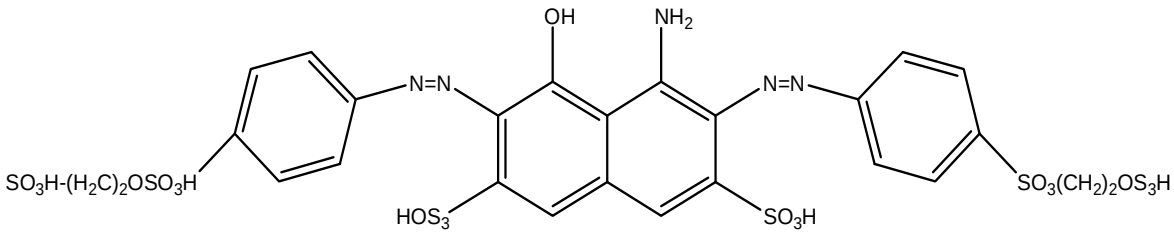

Fig .1 Estructura Química del NR5

2. Metodología Experimental

Materiales.

Los reactivos pirrol, NR5, persulfato de amonio, y celulosa fueron de la marca Sigma Aldrich (pureza > 99%), el $FeCl_2 \bullet H_2O$, $FeCl_3 \square 6H_2O$, y NaOH fueron adquiridos de Jalmek (pureza > 97%, México). En todos los experimentos se usó agua desionizada.

Síntesis de nanoparticulas de magnetita

Para la síntesis de la magnetita se adicionaron a un matraz volumétrico 1.987 g de $FeCl_2 \bullet 4H_2O$ y 5.406 g de $FeCl_3 \bullet 6H_2O$ en 100 mL de agua y se homogenizaron hasta su disolución. La solución homogénea se adicionó a un reactor de vidrio enchaquetado de 250 mL de capacidad a una velocidad de agitación de 300 rpm y se llevó a burbujeo constante con argón de ultra-alta pureza marca Infra^{MR} durante 1h para asegurar el desplazamiento

del oxígeno de la solución. En un sistema paralelo 3.2 g de NaOH se disolvieron en 100 mL de agua y se purgó con argón durante 1h. Posteriormente, la solución de NaOH se transfirió a una jeringa marca Hamilton-Gastithgt de vidrio de 100 ml y se colocó en una bomba de dosificación (KdScientific, Cole-Palmer^{MR}) a una velocidad de 2 mL/min, después de la adición de todo el NaOH. La reacción se llevó a cabo durante 3 h con agitación magnética. Al final, la mezcla obtenida se colocó en un vaso de precipitado de 500 mL y con un imán colocado debajo del vaso de precipitados se llevó a cabo la precipitación de las nanopartículas de magnetita. Una vez precipitadas las nanopartículas se hicieron los lavados de las partículas adicionando 200 mL de agua desionizada, este procedimiento se repitió 5 veces y se llevó a secado en una estufa a una temperatura de 60° C durante 24 horas.

Preparación del composito de α-celulosa /nanopartículas de magnetita/Polipirrol.

Para la síntesis del composito se dispersaron 5 g de α-celulosa en 50 mL de agua desionizada en un matraz Erlenmeyer de 125 mL. Al mismo tiempo en un vial se llevaron a dispersión las nanopartículas de magnetita previamente sintetizadas (1.0 g de nanopartículas de magnetita en 5 mL de agua) en un baño ultrasónico (Cole Parmer Instruments, CPX 130) durante 2 minutos con amplitud de 20%, potencia de 130 W y frecuencia de 20 Hz. Una vez sonicadas las nanopartículas se adicionaron a la dispersión acuosa de α-celulosa y se mantuvieron en agitación durante 5 min. Posteriormente, se añadieron a la mezcla 0.52 g de pirrol y se agitó durante otros 30 min. Después de este tiempo, se adicionaron 1.77 g de APS para iniciar la polimerización y se dejó reaccionar durante 2 h. El composito de α-celulosa/polipirrol/magnetita se colocó en un vaso de precipitado de 250 mL y se le adicionaron 50 mL de agua para su lavado y con ayuda de

un imán colocado en la parte inferior del vaso de precipitados se decantó el sobrenadante repitiendo los lavados 5 veces y se llevó a secado a 60°C durante 24 h.

Isotermas de adsorción y cinética.

Primeramente, se llevó a cabo la preparación de las soluciones con concentración de 20 a 200 mg/L de NR5 a 25°C. Se colocaron 25 mL de cada solución de colorante junto con 0.1 g de muestra en viales de 50 mL de capacidad, ajustando el pH a 3.0, 4.0 y 7 con NaOH o HCl 0.1M según fuera el caso. Los viales se mantuvieron en agitación constante durante 5 días para alcanzar el equilibrio. La adsorción en el equilibrio (q_e) se calculó mediante un balance de masa entre la concentración inicial y final del colorante en la solución.

Ecuación de balance de masa.

$$q = \frac{\mathrm{V}\ (\mathrm{Ci} - \mathrm{Cf})}{\mathrm{m}} \qquad (1)$$

Donde:

V = volumen de la solución en contacto con el adsorbente, (L)

Ci = concentración inicial de soluto en la solución, (mg/L)

Cf = concentración después del experimento, (mg/L)

m = masa de adsorbente, (g)

Las soluciones se analizaron en un espectrofotómetro UV/Vis (Thermo Scientific Evolution 220) a una λ=596 nm con una curva de calibración estándar de entre 10 y 300 mg/L. Los estudios de cinética de adsorción se corrieron de una manera similar a los de

equilibrio de adsorción pero muestreando a diferentes intervalos de tiempos de 0 a 25 horas.

Caracterización del material.

La α-celulosa y el composito de α-celulosa/magnetita/PPy fueron caracterizados mediante microscopia electrónica de barrido (JEOL, JSM 7800F). Estas muestras también fueron analizadas mediante FTIR (Cary 630, Agilent) y con un difractómetro de Rayos X (XRD) PANalytical Empyrean empleando la (λ = 1.54056 Å) a 40 kV y 40 mA. La comparación de picos entre la difracción experimental y la base de datos se hizo usando el software de difracción match 3. El área específica (A_{BET}) del composito se determinó mediante Fisisorción de N_2 (Micromeritics, ASAP 2020) usando el método de Brunauer-Emmett Teller (BET). La estabilidad térmica de la α-celulosa, magnetita, y el composito se estudiaron por análisis termogravimétrico (Setaram, Setsys Evolution) usando 10 mg de cada muestra que se calentó de 25 a 800 °C a una velocidad de calentamiento de 10°C/min. El punto de carga cero (PZC) se determinó por titulación: en un tubo nessler se colocó el volumen requerido de HCl o NaOH 0.1N para obtener un volumen final de 25 mL con un pH_0 en el intervalo de 1 a 12. Los tubos se mantuvieron en agitación constante durante 48 h. A la par se trabajó bajo las mismas condiciones, pero con la adición de 0.1g de muestra, después de 48 h se midió el pH_{of} final de la solución.

Modelo matemático

En este trabajo, el mecanismo de adsorción para el colorante NR5 en el composito fue descrito por el modelo matemático de tres resistencias (Montesinos et al. 2001) que estudia el mecanismo de transporte de las moléculas del colorante hacia el adsorbente, la difusión del colorante en los poros del composito, y la adsorción del colorante en la superficie de las partículas. El composito está conformado por núcleos de α-celulosa, donde se lleva a cabo la

difusión, y una delgada capa de nanopartículas de magnetita que se encuentra cubierta o inmersa en una matriz de PPy, donde ocurre el mecanismo de difusión y adsorción. Las ecuaciones descritas corresponden al modelo matemático sugerido por (Ovando-Medina. 2014) con la diferencia que esta vez se trabajó con la isoterma de Langmuir (aportando información del comportamiento electrónico). Las ecuaciones del modelo matemático se resolvieron por el método de líneas (Chapra et al. 2006). La coordenada radial fue discretizada usando el método de diferencias finitas de segundo orden (Geankoplis, 1983). La integración se discretizó por medio del integrador de ecuaciones ODE23 de Matlab®. Los datos obtenidos se emplearon en la estimación de los parámetros de la isoterma de adsorción. El coeficiente k_1, se estimó por ajuste experimental de datos de difusión del colorante con el software fminsearch de Matlab®. Ambas difusividades, D_0 y Di, fueron consideradas en un principio iguales por la simplicidad del modelo.

3. Resultados y Discusión

3.1 Caracterización del material.

En la Figura 2 se observan los espectros de FTIR de la α-celulosa, nanopartículas de magnetita, PPy y del composito. Los picos o bandas características correspondientes a estos compuestos se encuentran resumidos en la Tabla 1. Al analizar los espectros se observa que el espectro del composito es muy similar al de la celulosa a excepción de la banda de absorción en 1562 cm^{-1}; que está relacionada con la señal de vibración del enlace C=C del anillo aromático del polipirrol. El pico con la banda de absorción en 1458 cm^{-1} corresponde a la vibración de alargamiento del enlace C-C del anillo aromático del polipirrol (Ovando-Medina et al, 2014). La banda ancha de la Figura 2 correspondiente al

número de onda de 3300 cm^{-1}se asigna a la vibración de alargamiento del grupo OH de la celulosa, siendo esta banda no visible en el composito debido a la interferencia del polipirrol. Las bandas de 1046 y 1061 cm^{-1} corresponden al enlace C-O del enlace glucosídico de la celulosa, además se le asigna la banda de 1323 cm^{-1} a la vibración de flexión del grupo CH_2. En cuanto al pirrol se aprecian las bandas fundamentales en 1551y 1454 cm^{-1} correspondientes al estiramiento C-N del anillo aromático, observándose un desplazamiento hacia longitudes de onda de 1562 y 1458 cm^{-1} en el composito debido a la interacción entre los grupos OH de la celulosa y los grupos NH del pirrol (Johnston et al, 2006; Müller et al, 2011). En cuanto a la magnetita, suele presentar absorción en el infrarrojo a longitudes de onda entre 500 y 600 cm^{-1}, región del infrarrojo donde se presenta interferencia de ruido por lo que su análisis se determinó por medio de espectroscopia de rayos X.

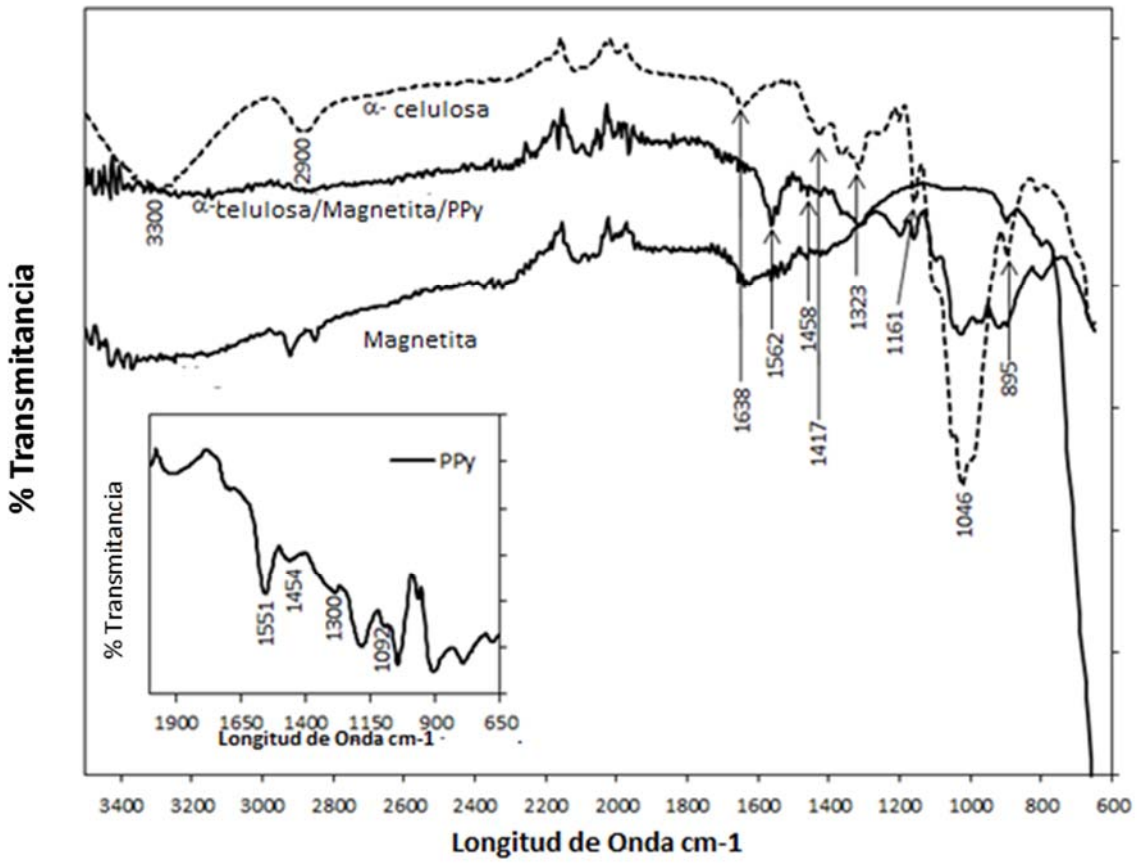

Fig. 2 Espectro de infrarrojo de α-Celulosa, Composito α-Celulosa Magnetita PPy, PPy y Magnetita.

Tabla 1. Señales de Infrarrojo para el pirrol y celulosa.

SEÑAL (cm^{-1})	PIRROL	SEÑAL (cm^{-1})	CELULOSA
1551	Estiramiento C=C	895	Estiramiento CO enlace β glucosídico
1454	Estiramiento C–C en el anillo	1046	Estiramiento CO del C6

1300	C–H en el plano.	1161	Estiramiento COC del enlace b-glucosídico.
1092	Vibración de alargamiento C–N	1323	Vibración de flexión del grupo CH_2
		1417	Doblamiento del enlace CH2 (sym) del C–6
		1638	Vibración de tensión de átomos de H vecinos
		2900	Estiramiento CH
		3300	Estiramiento OH

En La Figura 3 y 4 se pueden ver los difractogramas de rayos X de la magnetita y del composito α-celulosa/magnetita/PPy. En la Figura 3a se observan los picos característicos asociados con la estructura cubica Fe_3O_4 de la magnetita, los cuales coinciden con lo reportado en la base de datos 190629 PDF. Los picos principales para este tipo de estructura son debido a la difracción en el plano de 2Θ a (220), (311), (222), (400), (422), (511), (440), (531), (620), y (533) con picos alargados y de gran intensidad que corroboran la presencia de capas cristalinas. Por otra parte en la Figura 3a que corresponde al espectro de difracción de Rayos X del composito α-celulosa/magnetita/PPy sólo, es posible observar 3 picos anchos originados principalmente por la estructura amorfa del

PPy, el cual origina que sean imperceptibles los otros picos debido al recubrimiento de las partículas de magnetita y celulosa. De acuerdo con Kumar et al. (2014) el tipo de síntesis empleado determina el ángulo de difracción de la magnetita que va desde un 22° a 25° de 2θ (Su et al., 2012), en nuestro caso fue de 15°, 22.5°, y 35° de 2θ.

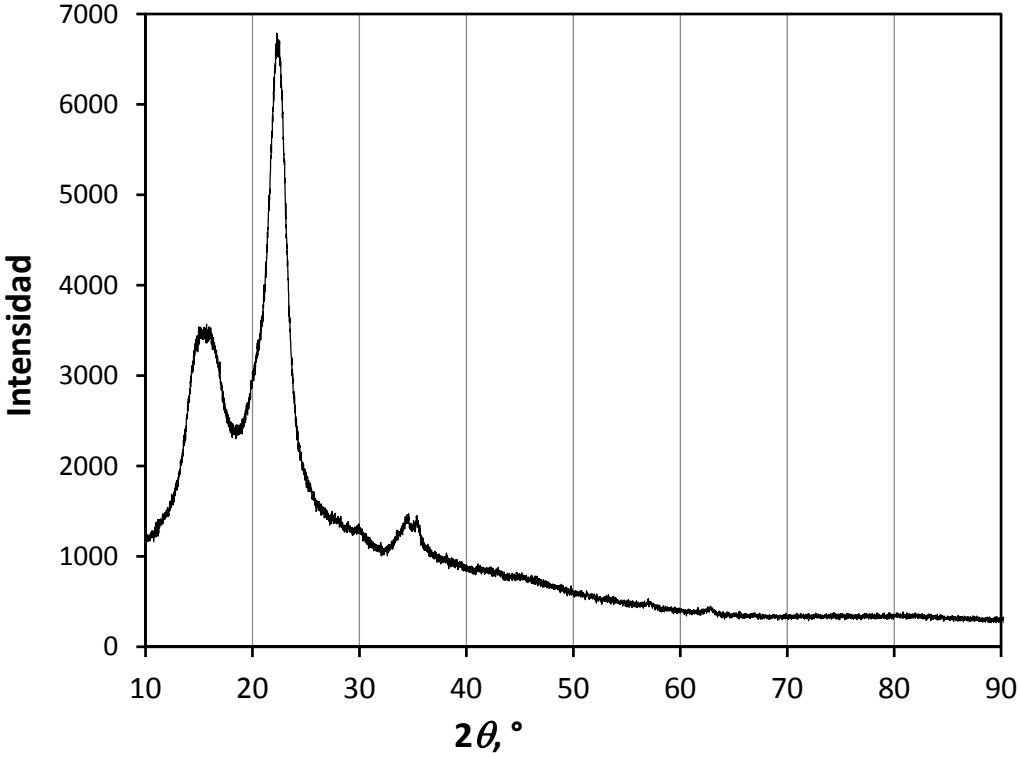

Fig. 3 Espectroscopia de Rayos X α-celulosa/magnetita/PPy

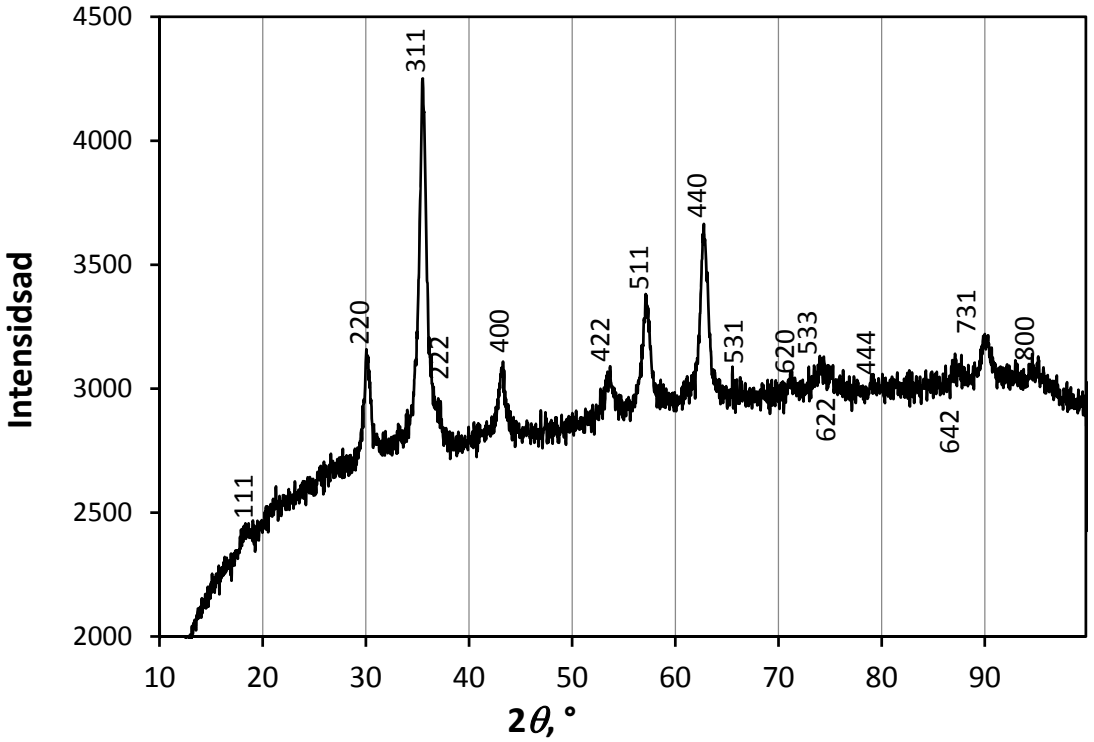

Fig. 4 Espectroscopia de Rayos X de magnetita

Las propiedades térmicas del material se pueden observar en la Figura 5 en donde se revela la gran estabilidad de la magnetita al presentar una pérdida de peso del 4% debido a su naturaleza inorgánica. La degradación de la α-celulosa se presenta alrededor de los 260°C. Sin embargo, la descomposición térmica del composito aparece a los 200°C muy probablemente debido a la degradación del polipirrol. En la figura se observa un intervalo de descomposición térmica del composito más lento debido principalmente a las nanopartículas de magnetita que intervienen en los enlaces formados entre la α-celulosa y polipirrol (Yang et al., 2007). Además, el composito muestra una pérdida de peso de un 87% (materia orgánica) a una temperatura mayor a los 550°C correspondiente al 11.3% de materia inorgánica de la magnetita y algunas cenizas de la α-celulosa y polipirrol. Mientras que para la celulosa existe una pérdida de peso de alrededor de un 96.5% del cual sólo un 3.5% corresponde a cenizas, se infiere que el composito contiene un 7.8% de nanopartículas de magnetita porcentaje menor al esperado del 20% empleado en la síntesis de la magnetita y se estima que solo un 23% de la α-celulosa se encuentra recubierta de polipirrol y magnetita.

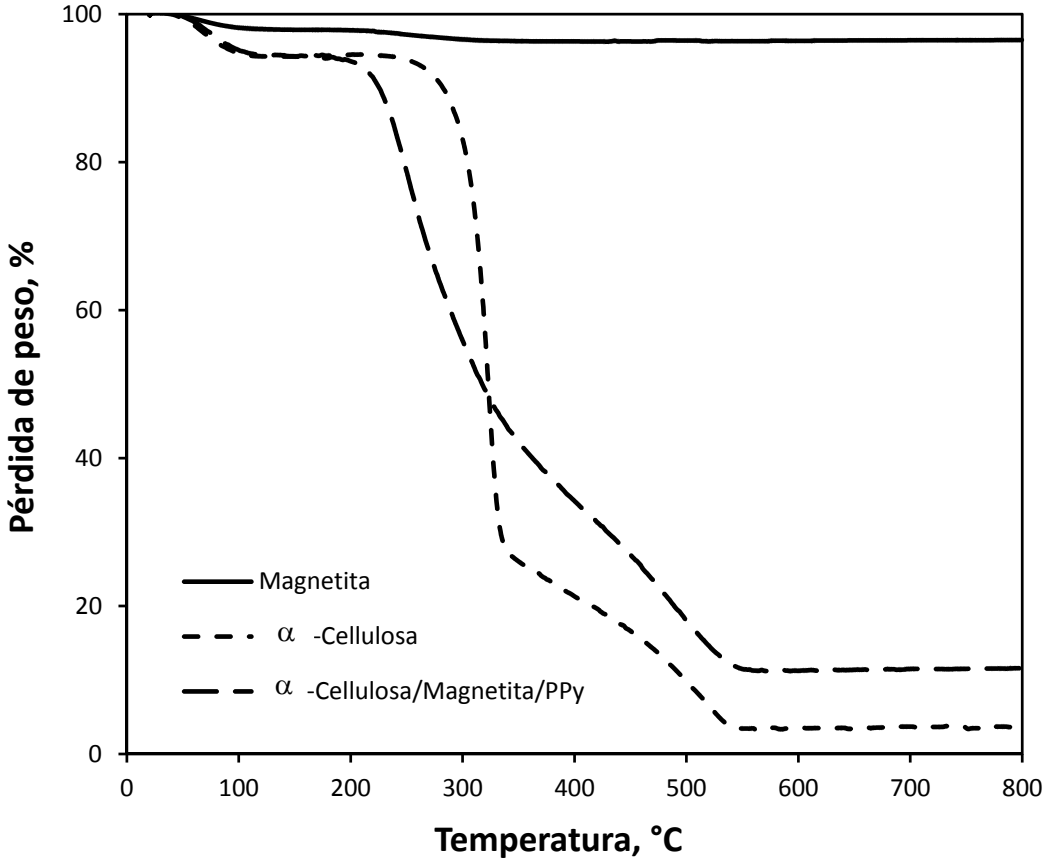

Fig. 5 Análisis Termogravimétrico de la α-celulosa/magnetita/PPy.

Las imágenes obtenidas por microscopia electrónica de barrido revelan fibras homogéneas y alargadas de la celulosa (Imagen 1a) que son muy similares a las reportadas por Ovando, (2014) en las que se observa que se encuentran recubiertas por partículas porosas de polipirrol (Imagen 1b) y nanopartículas de magnetita (Imagen 1c), las cuales están monodispersadas y con un diámetro promedio de 70 nm, para las posibles interacciones físicas, químicas y electrostáticas. Siendo este valor menor al reportado por Ovando, (2014) de 90 nm para partículas de celulosa recubiertas por polipirrol viéndose disminuido por la presencia de nanopartículas de magnetita.

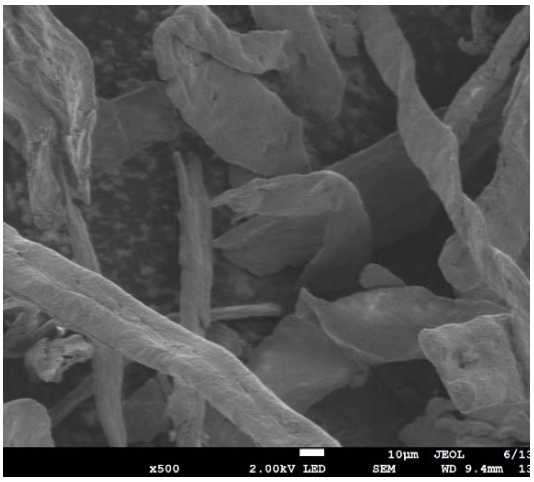

Imagen 1 (a) Celulosa

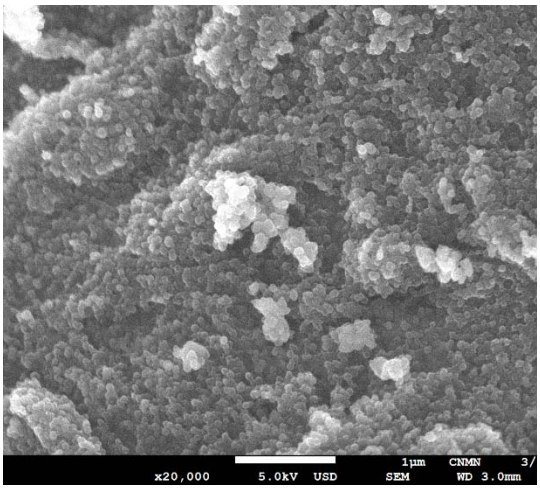

Imagen 1 (b) Celulosa

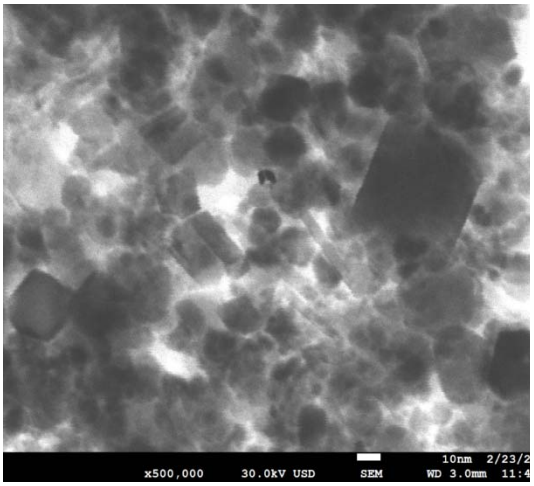

Imagen 1(c) magnetita

Imagen 1(d) composito con contraste

De la imagen 1(d) con contraste se realizó un análisis elemental (EDS) de esa área en específico para corroborar la presencia de magnetita en el composito haciendo la comparativa entre un área con magnetita Figura 7 y otra sin presencia de magnetita Figura 6. La composición química del área sin magnetita Tabla 2b) es de 50% de C, 48.48% de O, 0.48% de S y 0.77% de Fe, donde la presencia de impurezas como el S se deben principalmente al persulfato de amonio empleado en la polimerización del composito. En

contraparte la composición química del área en presencia de magnetita Tabla 2a) es de un 68.59% de Fe y 31.41% de O, correspondientes a la formula molecular de Fe_3O_4 de la magnetita con un radio atómico O/Fe de 1.6 nm el cual se encuentra dentro del rango reportado de 1.1 a 2.5 nm por (Bezdorozhev et al., 2017) y 20% mayor lo cual puede deberse a la presencia de los grupos OH ya que el tamaño final o individual de las partículas es afectado por varios parámetros como el pH de la solución, temperatura de reacción, concentración de los precursores e incluso una rápida o lenta agitación (Mascolo et al, 2013). Por ejemplo Goya et al, (2003) reportaron partículas de magnetita con un tamaño de 5 a 150 nm al precipitar partículas de hematita con $FeCl_3$ a 100°C durante 2 días en atmosfera de hidrogeno a 360°C.

La magnetita presenta una estructura cubica claramente observable en la Imagen 1(c) con partículas no muy homogéneas a simple vista pero al realizar el índice de polidispersión (Wm/Wn) Figura 5 arrojó un valor de 1.1 lo cual indica homogeneidad en las partículas, con un rango de diámetro de partícula de 7 a 18 nm y en promedio de 13nm muy similar a lo reportado de 9 a 14 nm.

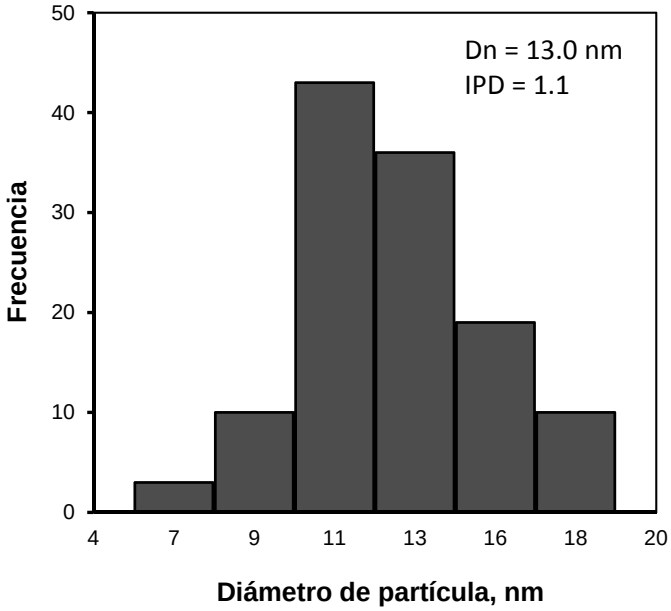

Fig. 5 Índice de polidespersión de la Magnetita.

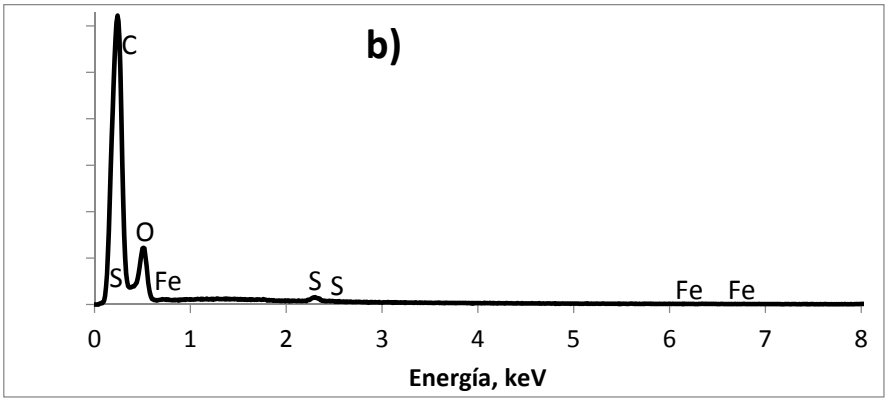

Fig. 6 Análisis Elemental del composito en ausencia de magnetita.

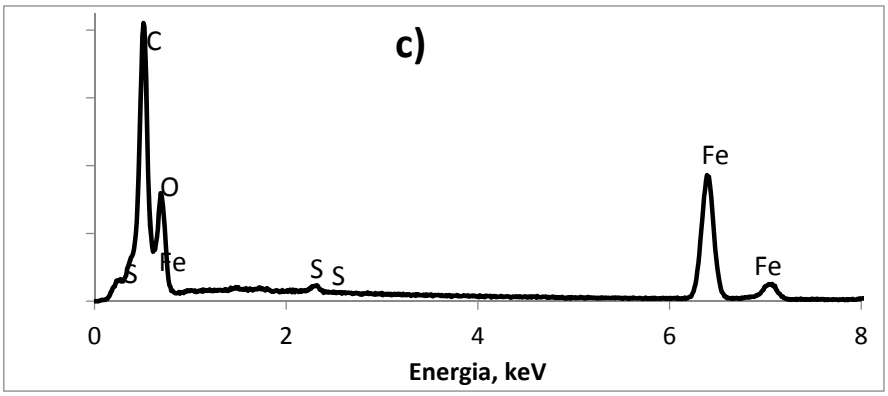

Fig. 7 Análisis Elemental del composito en presencia de magnetita.

Tabla. 2. Composición química del Composito.

Elemento	**Zona A**			**Zona B**		
	% Peso	% Atómico	%Error	% Peso	% Atómico	%Error
C *K*	69.6	75.5	4.0	-----	-------	------
O *K*	29.8	24.2	9.5	31.4	61.5	5.1
S *K*	0.4	0.1	7.1	-----	-------	---
Fe *K*	0.1	0.03	8.2	68.5	38.4	2.8

Cinética y Adsorción.

Las propiedades de adsorción de la superficie y la afinidad entre el adsorbato y el adsorbente fueron descritas por la isoterma de equilibrio de adsorción. El equilibrio se alcanza cuando la concentración del sorbato en la solución se encuentra en equilibrio dinámico con la concentración de la interface del adsorbente.

En este trabajo, los datos experimentales de la capacidad de adsorción en soluciones acuosas fueron descritos por el modelo de Langmuir y Freundlich.

Modelo de Langmuir:

$$Q_e = Q_m C_e/(1/K_L + C_e) \qquad (1)$$

Modelo de Freundlich:

$$Q_e = K_F(C_e)^n \qquad (2)$$

Donde Qe es la capacidad de adsorción en la concentración de equilibrio, *Ce e*s la constante de Langmuir (relacionada con la afinidad de los sitios activos), Q_m es la máxima capacidad de adsorción, K_F es la constante Freundlich, y *n* es la constante de heterogeneidad de la superficie del modelo de Freundlich.

Las constantes para estas isotermas fueron evaluadas por el método de mínimos cuadrados basado en la optimización de algoritmos. El porcentaje absoluto de la desviación promedio se calculó como sigue:

$$\%\, Desv = \frac{1}{n}\sum_0 i = N\ \frac{|Qexp - Qpred|}{Qpred}\ X\ 100 \qquad (3)$$

Donde N representa el número de datos, Q_{exp} la capacidad experimental de adsorción, y Qp_{red} predice los parámetros de adsorción. Los experimentos de adsorción para el composito α-celulosa /magnetita/PPy fueron descritos por el modelo de Freundlich y Langmuir a diferentes valores de pH mostrados en la Tabla 3. observándose, que el modelo de Langmuir fue el mejor descrito para la adsorción del colorante NR5.

La Figura 8 muestra la isoterma de adsorción (con base en la masa total del composito) del colorante NR5 en el composito α-celulosa/magnetita/PPy a pH 3.0, 4.0, y 7.0. Se puede apreciar en la Tabla 3 y Figura 8 que la máxima capacidad de adsorción decrece al aumentar los valores de pH. En otras palabras, la adsorción del colorante a pH ácido es mayor que a pH más alto. Este comportamiento puede ser explicado con el punto de carga cero (PZC) del composito que se muestra en la a Figura 8a. Cuando una superficie esta propensa a convertirse en carga positiva o negativa en función del pH y ese es el valor

de pH requerido para dar carga neta superficial cero, este valor se designa como el punto de carga cero (pcz). (Joong ,1989). El PZC fue de 1.2, lo que implica que la dispersión del composito se lleva a cabo a pH de 1.2; donde la suma de las cargas positivas y negativas son cero en la superficie del composito. A valores de pH más altos la superficie es predominantemente de carácter negativo. Se aprecia que tiene una carga casi neutra en un intervalo de pH de 1.2 a 3.2. Sin embargo si el pH incrementa por encima de 3.2 hasta alcanzar el valor de 9 la superficie adquiere una carga negativa. El colorante NR5 es una molécula de carácter aniónico que se disocia fácilmente en agua ver Figura 1; por consiguiente, las interacciones electrostáticas se favorecen entre el colorante y la superficie del composito a un pH por debajo de 3.2, donde el punto de carga cero es casi alcanzado. Por otra parte, es bien sabido que otros mecanismos físicos de adsorción pueden ocurrir.

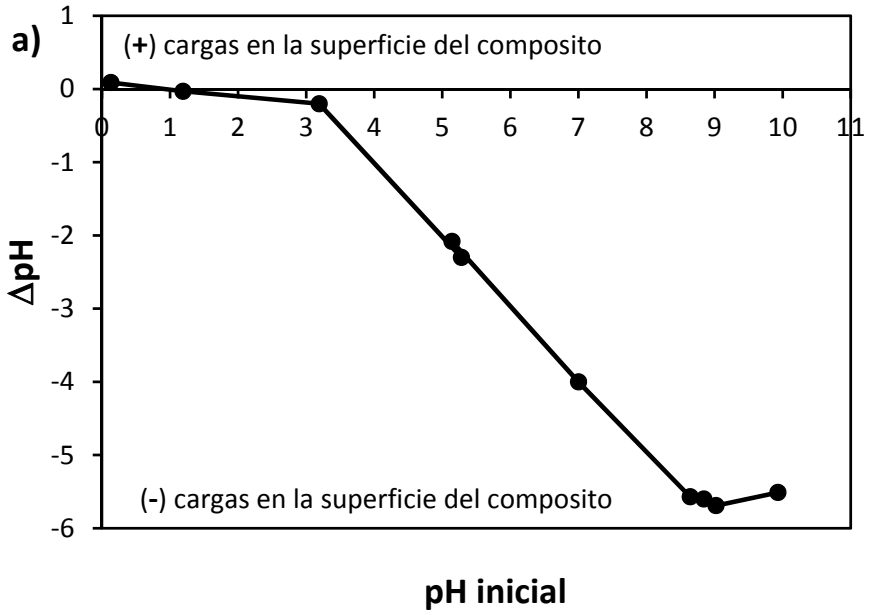

Fig. 8 a) Curva de carga de punto cero del composito sintetizado.

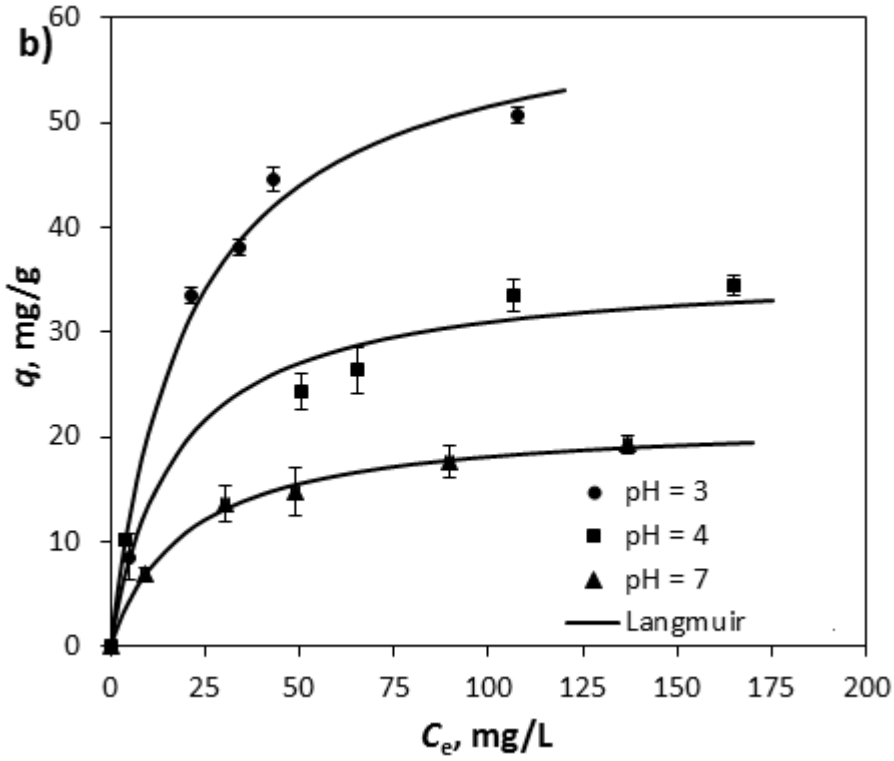

b) Isoterma de adsorción del composito α-celulosa /magnetita/PPy a diferentes valores de pH

Tabla 3. Parámetros de los modelos de Langmuir y Freundlich.

Modelo de Langmuir				
pH	**Qm mg/g**	**K_L mg^{-1}/l^{-1}**	**R^2**	**%D**
3	62.31	0.04	0.96	11.8
4	36.19	0.05	0.88	13.2
7	21.67	0.05	0.98	2.2
Modelo de Freundlich				
pH	**K_F $mg^{1-n}L^n$ g^{-1}**	**n**	**R^2**	**%D**

3	9.34	0.37	0.81	28.1
4	6.87	0.32	0.97	3.5
7	4.04	0.32	0.93	7.5

En la Figura 9 se observan los diferentes mecanismos de adsorción del Negro Reactivo 5 con el composito celulosa/magnetita/PPy donde existe una fuerte interacción π –π* entre los electrones del anillo aromático del colorante y los electrones π del anillo aromático del pirrol. Se observa la formación de un puente de hidrogeno entre el nitrógeno del pirrol y el nitrógeno del grupo amino del colorante, además pueden existir interacciones entre el átomo de oxígeno de la magnetita y el átomo de oxígeno de los grupos oxidrilo o el átomo de Nitrógeno del grupo azo del colorante a través de las moléculas de agua. Dato que se corrobora al determinar por medio del método de titulación de sitios activos, donde se obtuvo un valor de 1.97 meq/g para los sitios ácidos y 0.39 meq/g para los sitios básicos en el composito. La máxima adsorción se alcanzó en el pH = 3.0 y fue de 62.31 mg/g del composito, que corresponde a 0.25 meq/g de composito. Este valor es 7.8 veces más pequeño que el obtenido para los sitios activos ácidos, lo cual significa que no todos los sitios activos están disponibles para adsorción; sin embargo, es difícil discriminar con exactitud los mecanismos de adsorción. Es importante mencionar que el composito fue recuperado de la solución acuosa por medio de un imán; contribuyendo en la fácil aplicación y uso del composito.

Las concentraciones de los sitios activos en el composito se calcularon mediante la ecuación (4) siguiente:

$$C_{sa} = \frac{V_m(C_{in} - C_{fn})1000}{m} \qquad (4)$$

Donde:

C_{sa} = Concentración de sitios activos, meq/g

C_{in} = Concentración inicial de la solución neutralizante, eq/L

C_{fn} = Concentración final de la solución neutralizante, eq/L

M = Masa de FCA, g

V_{in} = Volumen inicial de la solución neutralizante, mL

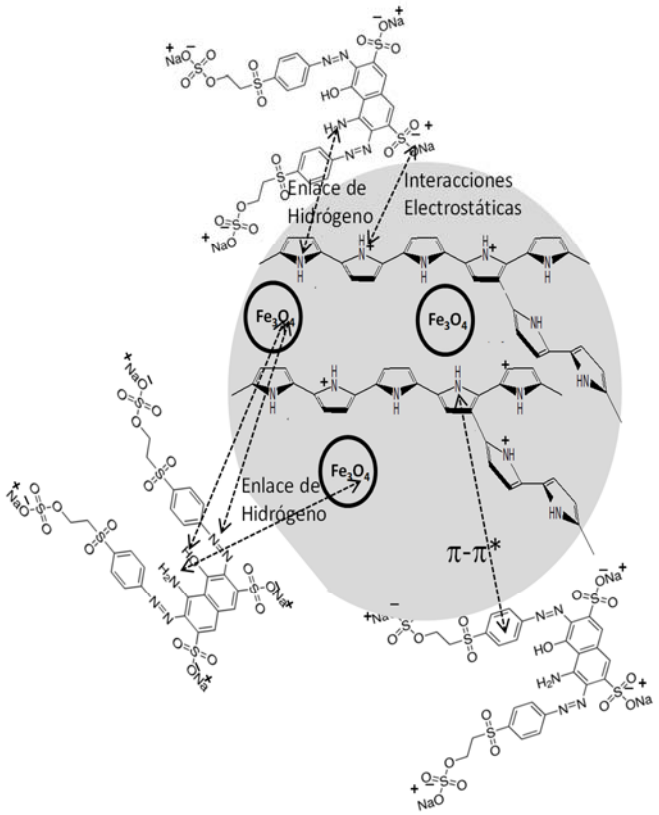

Fig. 9 Mecanismos de reacción entre el colorante y el composito.

La figura 10a muestra la curva de histéresis obtenida para el análisis de adsorción/desorción del N_2.donde se ve que la cantidad adsorbida de N_2 fue muy baja a los valores de presión relativa sometida. El fenómeno de histéresis se asocia con la condensación capilar en las estructuras con mesoporos. los diferentes tipos de curvas de histéresis son causadas de acuerdo al tipo de adsorbente y ambientes de sorción (como

temperatura y presión) (Qi et al,2017). De acuerdo con la IUPAC, la curva mostrada en la Figura 10a corresponde a una histéresis tipo H3 donde no hay presencia de microporos y no existe la tendencia para formar mesetas a presiones relativas bajas (Ballesteros et. 2014). El área BET (A_{BET}) del composito arrojó valores muy bajos (11.42 m^2/g), que puede deberse a que las partículas de celulosa se encuentran recubiertas por el polipirrol disminuyendo así el área específica del composito.

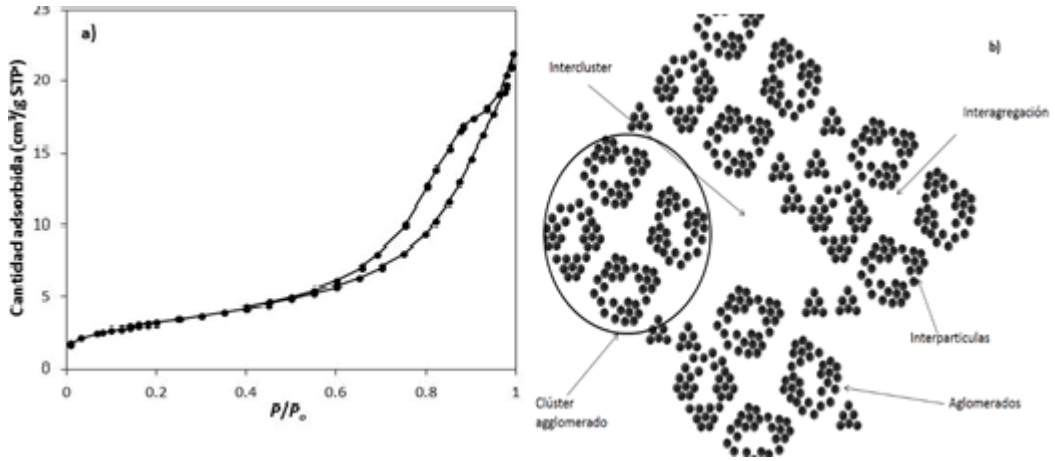

Fig. 10. (a) Curva de Histéresis de adsroción-desorción del N2 del composito. Fig 10(b) Estructura elemental y tipo de poros de las nanopartículas de magnetita y celulosa recubiertas por polipirrol.

Los datos experimentales y de simulación obtenidos en la cinética de adsorción para el colorante NR5 a pH 3.3 con 0.1 g de composito y 100 mg/L de concentración inicial del colorante se observan en la Figura 11. El coeficiente, k_1, se estimó adaptando el modelo matemático de tres resistencias a los datos experimentales obtenidos para el colorante empleando una concentración inicial de 100 mg/L. Luego, estos parámetros fueron optimizados para simular los datos de las condiciones siguientes. (La Tabla S1

de información electrónica suplementaria, que muestra los valores de los parámetros no graficados en las simulaciones). El valor usado en la densidad aparente(ρ_p) de las partículas adsorbentes fue de 1.46 g/mL siendo este el que mejor de adapta al modelo ver información complementaria, este valor generalmente se encuentran en un rango de 1.3 al 1.5 g/mL (Johnston et al 2006). La densidad de la capa porosa (ρo) fue de 1.45 g/mL para la celulosa (ε_i) valor que ya ha sido reportado anteriormente por Bhimte y Tayade (2007) mientras que para la película de magnetita (ε_0) se obtuvo de 0.35. De acuerdo con la Figura 11 se observa que el modelo matemático representa de manera efectiva los datos experimentales de la cinética de adsorción. Los valores estimados fueron para k_1 7.30×10-7 L/mg·s y 4.37×10^{-11} m^2 /s, respectivamente

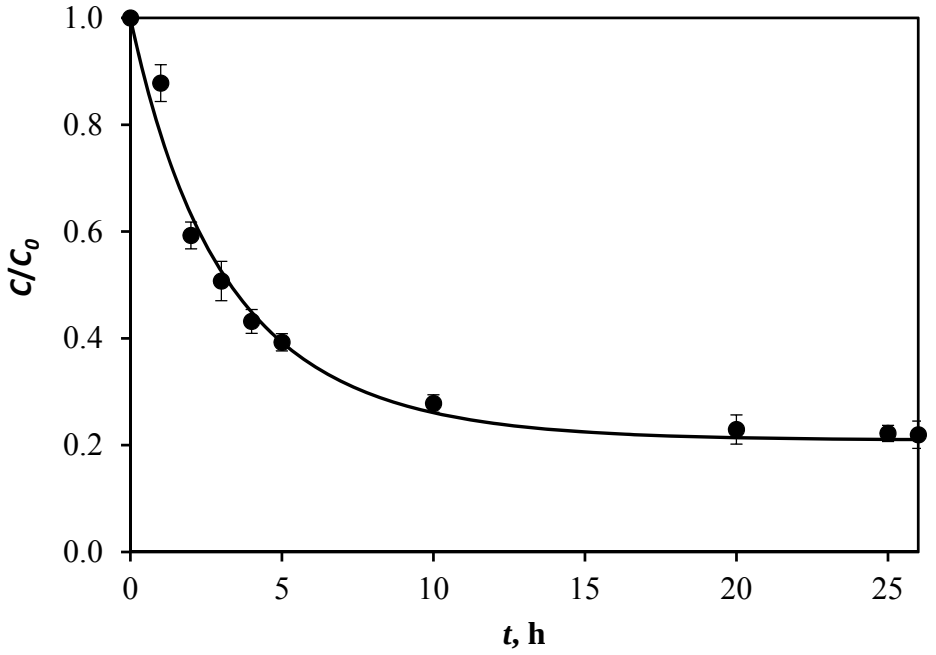

Fig. 11 Cinética de adsorción del NR5 a concentración inicial de 100 mg/L y 0.1g de composito y 70 rpm.

Es difícil llevar a cabo la comparación del coeficiente de adsorción con la información encontrada en literatura debido a que los modelos no cuentan con la información para describir la adsorción del colorante (Eren y Acar et al, 2006; Saha et al, 2011; Karadag et al, 2007) asimismo para los modelos de primer y segundo orden. Además,

estos modelos son sensibles a la concentración inicial del colorante y se requiere de hacer múltiples ajustes; estos modelos se basan en la concentración del colorante en el adsorbente descartando la resistencia en la transferencia de masas. Para evaluar la capacidad de predicción del modelo matemático, se corrieron 2 experimentos. Para la primera corrida la masa del composito (W_a) fue de 0.15g, la concentración inicial del colorante (C_A) 100 mg /L, y para la segunda corrida C_A y W_A *de* 50 mg/L y 0.1 g respectivamente. La Figura 12 muestra ambos resultados obtenidos en la experimentación donde se observa que el modelo matemático realiza una predicción del comportamiento de adsorción del colorante en el composito de estudio.

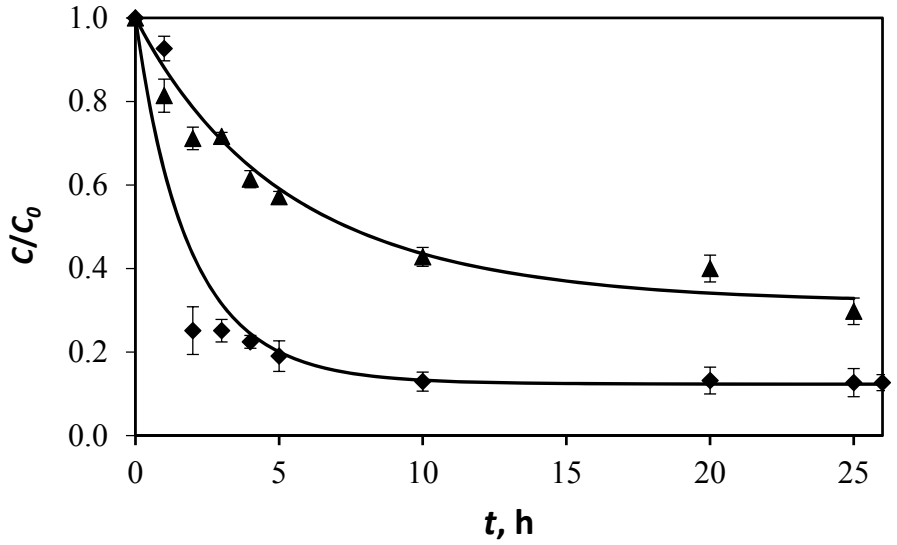

Fig. 12 cinética de adsroción del NR5 a concentración inicial de 50 mg/L y 0.1g de composito (diamantes) y CA=100Mg/L y 0.15g de composito (triángulos).

4. Conclusiones

Se sintetizó y caracterizó un composito de α-celulosa/nanoparticulas de magnetita/PPy. Se observó que la magnetita presentó la estructura cristalina cúbica correspondiente al Fe_3O_4, y una morfología irregular con un tamaño promedio monomodal

PSD de 13.0 nm. El composito se conforma por nanoparticulas de PPy con un tamaño aproximado de 70 de nm, recubriendo las fibras de celulosa y las nanopartículas de magnetita. El composito mostró un bajo valor de área específica A_{BET} de 11.4 m^2/g, que describe la presencia de mesoporos derivados de las interpartículas e incrustraciones del PPy. El composito mostró una gran capacidad de remoción del colorante NR5 en soluciones acuosas a pH ácido, la adsorción se derivó de las interacciones electrostáticas entre el colorante y la superficie cargada positivamente. El proceso de adsorción fue descrito por la isoterma de Langmuir con una capacidad máxima de adsorción de 62.3mg/g del colorante NR5. La cinética de adsorción del colorante NR5 fue bien descrita por el modelo matemático de tres resistencias, a valores de pH 3, Do 4.37×10^{-11} m^2/s y k_1 de $7.30\times^{10\text{-}7}$ L/mg·s.

Referencias

1. Informe Mundial de las Naciones Unidas de Desarrollo del agua 2017 (2017). Agua residual: El Recurso Inexplotado The United Nations World Water Development Report 2017 (2017)., Paris. http://unesdoc.unesco.org/images/0024/002475/247552e.pdf. publicado 21 Julio del 2017.
2. Water and wastewater International: textile dyeing without effluent. http://www.waterworld.com/articles/wwi/2017/02/case-study-textile-dyeing-without-effluent.html (2017). Publicado agosto 2 Augusto del 2017.
3. B.H. Hameed, D.K. Mahmoud, A.L. Ahmad, Equilibrium modeling and kinetic studies on the adsorption of basic dye by a low-cost adsorbent: Coconut (Cocos nucifera) bunch waste, J. Hazard. Mater., 158 (2008) 65–72.
4. I.A.W. Tan, A.L. Ahmad, B.H. Hameed, Adsorption of basic dye on high-surface-area activated carbon prepared from coconut husk: Equilibri, kinetic and thermodynamic studies, J. Hazard. Mater., 154 (2008) 337–346.
5. B. Noroozi, G.A. Sorial, H. Bahrami, M. Arami, Equilibrium and kinetic adsorption study of a cationic dye by a natural adsorbent—Silkworm pupa, J. Hazard. Mater., 139 (2007) 167–174.
6. K.Y. Hor, J.M.C. Chee, M.N. Chong, B. Jin, C. Saint, P.E. Poh, R. Aryal, Evaluation of physicochemical methods in enhancing the adsorption performance of natural zeolite as low-cost adsorbent of methylene blue dye from wastewater, J. Clean. Prod. 118 (2016) 197–209.

7. O.A. Saputra, M.D. Prameswari, V.T.D. Kinanti, O.D. Mayasari, Y.D. Sutarni, K. Apriany, W.W. Lestari, Preparation, characterization and methylene blue dye adsorption ability of acid activated-natural zeolite, OP Conf. Ser.: Mater. Sci. Eng., (2017) https://doi.org/10.1088/1757-899X/172/1/012039
8. I. Humelnicu, A. Băiceanu, M.-E. Ignat, V. Dulman, The removal of Basic Blue 41 textile dye from aqueous solution by adsorption onto natural zeolitic tuff: Procesos cinéticos y termodinamicos,. Saf. Environ. Prot., 105 (2017) 274–287.
9. R. Aziam, M. Chiban, E. Eddaoudi, A. Soudani, M. Zerbet, F. Sinan, Factors controlling the adsorption of acid blue 113 dye from aqueous solution by dried C. edulis plant as natural adsorbent, Arab. J. Geosci., (2016) https://doi.org/10.1007/s12517-016-2675-4
10. A. Pérez-Escobedo, P.E. Díaz-Flores, J.R. Rangel-Méndez, F.J. Cerino-Cordova, V.M. Ovando-Medina, J.A. Alcalá-Jáuregui, Fluoride adsorption capacity of composites based on chitosan-zeolite-algae, Rev. Mex. Ing. Quím., 15 (2016) 139–147.
11. U. Habiba, T.A. Siddique, T.C. Joo, A. Salleh, B.C. Ang, A.M. Afifi, Synthesis of chitosan/polyvinyl alcohol/zeolite composite for removal of methyl orange, Congo red and chromium(VI) by flocculation/adsorption, Carbohyd. Polym., 157 (2017) 1568–1576.
12. H. Wang, T. Lin, A. Kaynak, Polypyrrole nanoparticles and dye absorption properties, Synth. Met. 151 (2005) 136–140.
13. V.M. Ovando-Medina, P.E. Díaz-Flores PE, H. Martínez-Gutiérrez, L.A. Moreno-Ruiz, Antonio-I.D. Carmona, M. Hernández-Ordoñez, Composite of cellulosic

agricultural waste coated with semiconducting polypyrrole as potential dye remover, Polym. Compos., 35 (2014) 186–193.

14. M. Banimahd-Keivani, K. Zare, H. Aghaie, R. Ansari, Removal of methylene blue dye by application of polyaniline nano composite from aqueous solutions, J. Phys. Theor. Chem. IAU Iran, 6 (2009) 63–70.
15. R. Ansari, Z. Mosayebzadeh, Removal of basic dye methylene blue from aqueous solutions using sawdust and sawdust coated with polypyrrole, J. Iran. Chem. Soc., 7 (2010) 33–35.
16. V.M. Ovando-Medina, J. Vizcaíno-Mercado, O. González-Ortega, J.A. Rodríguez de la Garza, H. Martínez-Gutiérrez, Synthesis of α-cellulose/polypyrrole composite for the removal of reactive red dye from aqueous solution: Kinetics and equilibrium modeling, Polym. Compos. 36 (2015) 312–321.
17. A.R. Bagheri, M. Ghaedi, A. Asfaram, A.A. Bazrafshan, R. Jannesar, Comparative study on ultrasonic assisted adsorption of dyes from single system onto Fe_3O_4 magnetite nanoparticles loaded on activated carbon: Experimental design methodology, Ultrason. Sonochem., 34 (2017) 294–304.
18. L. Bai, Z. Li, Y. Zhang, T. Wang, R. Lu, W. Zhou, H. Gao, S. Zhang, Synthesis of water-dispersible graphene-modified magnetic polypyrrole nanocomposite and its ability to efficiently adsorb methylene blue from aqueous solution, Chem. Eng. J., 279 (2015) 757–766.
19. M. Ayad, N. Salahuddin, A. Fayed, B.P. Bastakoti, N. Suzuki, Y. Yamauchi, Chemical design of a smart chitosan–polypyrrole–magnetite nanocomposite toward efficient water treatment, Phys. Chem. Chem. Phys., 16 (2014) 21812-21819.

20. A.A. Asgharinezhad, H. Ebrahimzadeh, Coextraction of acidic, basic and amphiprotic pollutants using multiwalled carbon nanotubes/magnetite nanoparticles@polypyrrole composite, J. Chromatogr. A, 1412 (2015) 1–11.
21. R.M. Montesinos, R. Guzmán, A. Tejeda-Mansir, Simulation of stirred tank affinity processes applied to separation of proteins, Int. J. Bio-Chromatogr., 6 (2001) 231–243.
22. S. Chapra, R. Canale, Numerical methods for engineers, McGraw-Hill, New York, 1983.
23. C.J. Geankoplis, Transport processes and unit operations, Allyn and Bacon, Boston, 1983.
24. J.I, Morán, V.A. Alvarez, V.P. Cyras, A. Vázquez, Extraction of cellulose and preparation of nanocellulose from sisal fibers, Cellulose, 15 (2008) 149–159.
25. X. Li, L.G. Tabil, S. Panigrahi, Chemical treatments of natural fiber for use in natural fiber-reinforced composites: A review, J. Polym. Environ., 15 (2007) 25–33.
26. J.H. Johnston, F.M. Kelly, J. Moraes, T. Borrmann, D. Flynn, Conducting polymer composites with cellulose and protein fibres, Curr. Appl. Phys., 6 (2006) 587–590.
27. D. Müller, C.R. Rambo, D.O.S. Recouvreux, L.M. Porto, G.M.O. Barra, Chemical in situ polymerization of polypyrrole on bacterial cellulose nanofibers, Synth. Met. 161 (2011) 106–111.
28. N. Su, H.B. Li, S.J Yuan, S.P. Yi, E.Q. Yin, Synthesis and characterization of polypyrrole doped with anionic spherical polyelectrolyte brushes, Express Polym. Lett. 6 (2012) 697–705.

29. A. Kumar, Y.S. Negi, V. Choudhary, N.K. Bhardwaj, Characterization of cellulose nanocrystals produced by acid-hydrolysis from sugarcane bagasse as agro-waste, J. Mat. Phys. Chem., 2 (2014) 1–8.
30. M.C. Mascolo, Y. Pei, T.A. Ring, Room temperature co-precipitation synthesis of magnetite nanoparticles in a large pH window with different bases, Materials, 6 (2013) 5549–5567.
31. G.F. Goya, T.S. Berquó, F.C. Fonseca, Static and dynamic magnetic properties of spherical magnetite nanoparticles, J. Appl. Phys., 94 (2003) 3520–3528.
32. S. Sun, H. Zeng, Size-controlled synthesis of magnetite nanoparticles, J. Am. Chem. Soc. 124 (2002) 8204–8205.
33. J.H. Johnston, J. Moraes, T. Borrmann, Conducting polymers on paper fibres, Synth. Met. 153 (2005) 65–68.
34. G. Nyström, A. Mihranyan, A. Razaq, T. Lindström, L. Nyholm, M. Strømme, A Nanocellulose polypyrrole composite based on microfibrillated cellulose from wood, J. Phys. Chem. B, 114 (2010) 4178–4182.
35. M. Wawrzkiewicz, Z. Hubicki, In: A. Kilislioglu, Ion Exchange - Studies and Applications, InTech, pp. 37–72.
36. L. Qi, X. Tang, Z. Wang, X. Peng, Pore characterization of different types of coal from coal and gas outburst disaster sites using low temperature nitrogen adsorption approach, Int. J. Mining Sci. Tech., 27 (2017) 371–377.
37. L.F. Ballesteros, J.A. Teixeira, S.I. Mussatto, Chemical, functional, and structural properties of spent coffee grounds and coffee silverskin, Food Bioprocess Tech., 7 (2014) 3493–3503.

38. N.A. Bhimte, P.T. Tayade, Evaluation of microcrystalline cellulose prepared from sisal fibers as a tablet excipient: a technical note. AAPS Pharm. Sci. Tech. 8 (2007) E56–E62.
39. Z. Eren, F.N. Acar, Adsorption of reactive black 5 from an aqueous solution: equilibrium and kinetic studies, Desalination ,194 (2006) 1–10.
40. T.K. Saha, N.C. Bhoumik, S. Karmaker, M.G. Ahmed, H. Ichikawa, Y. Fukumori, Adsorption characteristics of reactive black 5 from aqueous solution onto chitosan, CLEAN–Soil, Air, Water, 39 (2011) 984–993.
41. D. Karadag, M. Turan, E. Akgul, S. Tok, A. Faki, Adsorption equilibrium and kinetics of reactive black 5 and reactive red 239 in aqueous solution onto surfactant-modified zeolite, J. Chem. Eng. Data, 52 (2007) 1615–1620.

Synthesis of α-cellulose/magnetite/polypyrrole composite for the removal of reactive black 5 dye from aqueous solutions

Journal:	*Desalination and Water Treatment*
Manuscript ID	TDWT-2018-1464
Manuscript Type:	Original Paper
Date Submitted by the Author:	29-Jul-2018
Complete List of Authors:	Ovando-Medina, Victor; Universidad Autonoma de San Luis Potosi, Cordinacion Academica Region Altiplano Guzman, Camerina; Universidad Autonoma de San Luis Potosi, Cordinacion Academica Region Altiplano Diaz-Flores, Paola E.; Universidad Autonoma de San Luis Potosi, Martínez-Gutiérrez, Hugo; Centro de Nanociencias y micro y nanotecnologías, Instituto Politécnico Nacional Gonzalez, Omar; Universidad Autonoma de San Luis Potosi, Facultad de Ciencias Químicas
Keywords:	Cellulose, magnetite nanoparticles, polypyrrole, dye adsorption, composite

Synthesis of α-cellulose/magnetite/polypyrrole composite for the removal of reactive black 5 dye from aqueous solutions

Víctor M. Ovando-Medina[1*], Camerina J. Guzmán-Álvarez[1], Paola E. Díaz-Flores[2], Hugo Martínez-Gutiérrez[3], Omar González-Ortega[4]

[1] Ingeniería Química, Coordinación Académica Región Altiplano (COARA), Universidad Autónoma de San Luis Potosí. Carretera a Cedral KM 5+600, San José de las Trojes, Matehuala, San Luis Potosí 78700, México. Email: ovandomedina@yahoo.com.mx, phone: +528442245572

[2] Facultad de Agronomía, Universidad Autónoma de San Luis Potosí. Km. 14.5 Carretera San Luis Potosí-Matehuala, Ejido Palma de la Cruz, Soledad de Graciano Sánchez, San Luis Potosí, Apdo. Postal 32,78321, México. Email: paola.diaz@uaslp.mx, phone: +524441713818

[3] Centro de Nanociencias y Micro y Nanotecnologías, Instituto Politécnico Nacional (IPN). Luis Enrique Erro S/N, D.F. 07738, México. Email: hamartinez63@hotmail.com, phone: +525545664446

[4] Facultad de Ciencias Químicas, Universidad Autónoma de San Luis Potosí. Av. Dr. Manuel Nava No.6, Zona Universitaria, San Luis Potosí, S.L.P. 78210, México. Email: omar.gonzalez@uaslp.mx, phone: +524442912743

Abstract

A composite was obtained from α-cellulose coated with magnetite nanoparticles and conducting polypyrrole (PPy). The magnetite nanoparticles were synthesized by the coprecipitation method from $FeCl_2$ and $FeCl_3$ salts. The composite was obtained by pyrrole polymerization in the presence of a mixture of α-cellulose and magnetite nanoparticles. The magnetite nanoparticles and composite were characterized by FTIR and UV/Vis-NIR spectroscopies, scanning electron microscopy (SEM), energy dispersive spectroscopy (EDS), X-ray diffraction (XRD), and thermogravimetric analyses (TGA). XRD analysis demonstrated that magnetite nanoparticles with the typical cubic structures of Fe_4O_3 were obtained. SEM analysis showed that magnetite nanoparticles had irregular morphology with average size of 13 nm, whereas the composite consisted of

spherical nanoparticles of PPy coating α-cellulose fibers and magnetite nanoparticles. Batch aqueous adsorption experiments of the reactive black 5 (RB5) dye onto the synthesized material were conducted. The results showed that for the adsorption experiments set to initial pH of 3.0, the maximum adsorption capacity was 62.31 mg of dye/g of composite while a value of 21.67 mg of dye/g of composite was obtained when the initial solution pH was set to 7.0. Adsorption isotherms for the RB5 dye were well described by the Langmuir model. The transient adsorption process of the RB5 dye onto the composite was described by a general three-resistance model, allowing the estimation of the effective diffusivity, D_0, and the adsorption rate coefficient, k_1. For the adsorption experiments with an initial pH value set to 3.0, D_0 was estimated as 4.37×10^{-11} m^2/s while k_1 was 7.30×10^{-7} L/mg·s.

Keywords: *cellulose; magnetite nanoparticles; polypyrrole; dye adsorption; composite*

1. Introduction

According to the 2017 UN World Water Development Report, anthropological activities use water and generate wastewater. Due to the increasing water demand, the quantity of wastewater produced and its overall pollution load are continuously increasing. Over 80% of the wastewater generated worldwide and over 95% in some undeveloped countries is released to the environment without any treatment. Wastewater is usually discarded into water bodies, diluted or transported downstream, or it infiltrates into aquifers; affecting the quality of freshwater supplies [1].

The textile and leather industries are high water demanding whose effluents are severely polluted. Therefore wastewater treatment is a global challenge for scientists and governments and at the same time an attractive growth market for industries developing water purification technologies. For example, the market for reverse osmosis membrane elements is currently projected to grow at an above-average rate of 10% annually in the coming three years. In the case of ion exchange resins, future growth is predicted to average 4% per year [2].

In the development of new adsorbent materials; it is important to consider several factors such as raw materials availability, simple synthesis, low cost, reusability, and recovery. In this regard different materials have been prepared and studied as natural adsorbents such as coconut fibers waste [3], activated carbon from coconut husk [4], silkworm pupa [5], natural zeolites [6-8], and plants [9]. However, it has been observed

that composites of two or more natural adsorbents or natural absorbents with synthetic polymers can improve the removal efficiency of different dyes from wastewater. For example, our group recently reported the use of chitosan/zeolite and chitosan/algae composites for fluoride adsorption from aqueous solutions. We observed that at pH 5 the chitosan/zeolite composite had a 1.2-fold increase in fluoride adsorption when compared to the chitosan/algae composite, which showed a higher capacity for fluoride removal at pH 7 [10]. Habiba et al. [11] prepared a composite of chitosan/polyvinyl alcohol/zeolite for the removal of methyl orange and congo red dyes through coagulation and adsorption processes, observing good composite performance in the contaminants removal.

The preparation of composites with natural adsorbents and synthetic polymers has been of increasing interest since natural absorbents are usually of low cost provided they can be originated from wastes (e.g. lignocellulosic materials) or by-products. Moreover, natural adsorbents can be easily combined with small amounts of synthetic polymers; which confer better adsorption properties. Particularly, the conducting polymers PPy and polyaniline are of interest due to their good environmental stability, simple synthesis, and high electrical conductivity [12]. On this sense, we reported the preparation of sorghum/PPy composite from sorghum sub-product (cellulosic fibers from stalks) and semiconducting PPy obtained by chemical oxidizing polymerization. This composite was used for the removal of methylene blue dye from aqueous solutions; obtaining a maximum adsorption capacity of 143.5 mg/g (66.4% more than sorghum fibers alone) [13]. A similar work was reported by Ansari and coworkers [14] who prepared a composite of sawdust from walnut tree and polyaniline; they used it to adsorb methylene blue dye from aqueous solutions at room temperature and pH 9. From their reported Langmuir isotherm data; the maximum adsorption capacity was 8.3 mg/g. However when using PPy instead of polyaniline; the maximum adsorption capacity increased to 34.3 mg/g [15]. More recently, we used a composite of α-cellulose/PPy for the removal of the reactive red 120 dye from aqueous solutions. We observed a maximum adsorption capacity of 96.1 mg/g at acidic pH [16].

Thus, the combination of natural adsorbents and semiconducting polymers increases dye adsorption capacity. However from a practical point of view, adsorbent recovery after dye adsorption is very important since the saturated adsorbent has to be disposed or regenerated for reuse. One option to overcome this recovery problem is the synthesis or preparation of materials with magnetic properties that can be separated using external magnetic fields. Today, researchers are paying attention to the synthesis of iron-based magnetic nanoparticles due to their particular structure and properties; which allow their application in several

chemistry and engineering fields. Compared to their atomic or bulky counterparts; Fe_3O_4 nanoparticles have superior physical and chemical properties due to their mesoscopic effect, small object effect, quantum size effect, surface effect, superparamagnetic character, and non-toxic properties [17]. Some results about the preparation of composites based on PPy and magnetite were reported by Bai et al. [18], who prepared a nanocomposite of water-dispersible graphene-modified magnetic polypyrrole (Fe_3O_4/PPy/RGO) and studied its ability in the methylene blue dye adsorption from aqueous solution. These authors observed a maximum methylene blue adsorption capacity for the composite of 270.3 mg/g with a Langmuir isotherm. In another work, Ayad et al. [19] reported the synthesis of chitosan/PPy/magnetite nanocomposite for the removal of acid green 25 dye; observing high adsorption capacity when compared to PPy and chitosan alone. The magnetic properties of the composites allowed their recovery at the end of the adsorption process. Asgharinezhad et al. [20] used a composite of multi-walled carbon nanotubes/magnetite nanoparticles/PPy in the co-extraction of acidic, basic, and amphiprotic pollutants (polar and nonpolar).

The purpose of the present work was to prepare and characterize a composite of α-cellulose coated with magnetite nanoparticles and the semiconducting PPy. This composite was used in the removal of the anionic reactive black 5 (RB5) dye (Figure 1) from aqueous solutions. A general three-resistance mathematical model was used to describe the adsorption mechanism of the dye onto the surface of the synthesized composite.

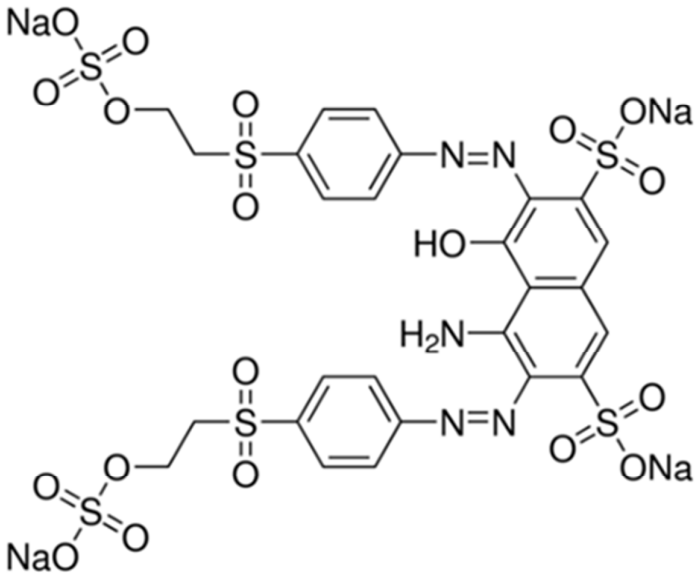

Fig. 1 Chemical structure of the reactive black 5 (RB5) dye

2. Experimental

Materials

Pyrrole monomer, reactive black 5 dye, ammonium persulfate, and α-cellulose were purchased from Sigma-Aldrich (>99%) and used as received. $FeCl_2 \bullet 4H_2O$, $FeCl_3 \bullet 6H_2O$, and NaOH were acquired from Jalmek (>97%, Mexico). Deionized water was used in all experiments.

Magnetite nanoparticles synthesis

In 100 mL of deionized water; 0.01 mol (1.987 g) of $FeCl_2 \bullet 4H_2O$ and 0.02 mol (5.406 g) of $FeCl_3 \bullet 6H_2O$ were dissolved. This solution was charged to a 250 mL three-neck glass jacketed reactor with mechanical stirring (300 rpm). The mixture was bubbled with argon of ultra-high purity from Infra™ for 1 h to displace dissolved oxygen. In the meantime, 0.08 mol (3.2 g) of NaOH were dissolved in 100 mL of water and purged with argon for 1 h. Afterwards the NaOH solution was transferred to a 100-mL syringe (Hamilton-Gastight), mounted on an addition pump (KdScientific, Cole-Parmer™), and added to the reactor at a rate of 2 mL/min. After NaOH addition, the reaction was allowed to proceed for 3 h. Subsequently the reaction mixture was poured into a 500 mL-beaker, a magnet was placed under the beaker to precipitate the magnetite nanoparticles; the supernatant was discarded. Afterwards, 200 mL of deionized water were added to the magnetite nanoparticles and the precipitation procedure was repeated. This washing process was repeated five times to remove unreacted material. The washed magnetite nanoparticles were dried at 60 °C for 24 h.

α-Cellulose/Magnetite nanoparticles/Polypyrrole composite preparation

5 g of α-cellulose were dispersed in 50 mL of deionized water in a 125-mL Erlenmeyer flask. In a vial, 1.0 g of magnetite nanoparticles were dispersed in 5 mL of water and immersed into an ultrasonic bath for 2 min to disperse the nanoparticles. Later, the sonicated magnetite nanoparticles dispersion was added to the aqueous α-cellulose dispersion and the mixture was stirred for 5 min. Afterwards 0.52 g of pyrrole monomer were added, and the mixture was stirred for 30 min. Subsequently 1.77 g of APS were added to start the polymerization process. The reaction was allowed to proceed for 2 h. The resulting composite was precipitated using a magnet placed under the reaction flask and the supernatant was decanted. 50 mL of water

were then added, the composite was precipitated again with the magnet, and supernatant was decanted. This washing procedure was repeated five times. The washed composite was dried at 60 °C for 24 h.

Adsorption isotherms and kinetics determination

Batch adsorption experiments were performed at 25 °C at initial pH values set to 3.0, 4.0, and 7.0 as follows: 0.1 g of composite were added to a glass vial along with 30 mL of a RB5 dye solution of known concentration in the range from 20 to 200 mg/L. The pH was adjusted using 0.01 M HCl or NaOH. Vials were continuously stirred using an orbital shaker at constant temperature for 5 days. Adsorbed dye concentration at equilibrium (q_{oe}) was calculated by a mass balance using the initial and final dye concentrations in solution. Concentrations of the RB5 dye throughout the adsorption experiments were determined using a spectrophotometer set to λ = 596 nm (Thermo Scientific, Evolution 220) with a calibration curve constructed with standard solutions in the range from 10 to 300 mg/L. Adsorption kinetics experiments were run similarly to the equilibrium studies but determining dye solution concentrations at different times.

Material characterization

The uncoated α-cellulose and the α-cellulose/magnetite nanoparticles/PPy composite were characterized by scanning electron microscopy (JEOL, JSM 7800F). These samples were also analyzed by FTIR with ATR (Cary 630, Agilent) and X-Ray diffraction (XRD) with a PANalytical Empyrean diffractometer using the $Cu_{K\alpha}$ radiation (λ = 1.54056 Å) at 40 kV and 40 mA. The correspondence between the experimental diffraction peaks and the powder diffraction file (PDF) database position was made using the Match! 3 phase identification from powder diffraction software. The specific surface area (A_{BET}) of the composite was determined by N_2 physisorption (Micromeritics, ASAP 2020) using the Brunauer-Emmett-Teller (BET) method. Thermal stability of pure α-cellulose, magnetite, and composite was studied by thermogravimetric analysis (Setaram, Setsys Evolution) using 10 mg of each sample that was heated from 25 to 800 °C at a heating rate of 10 °C/min. Point of zero charge (PZC) was determined by titration as follows: in a conical vial the required volume of 0.1 M HCl or NaOH solution was mixed with the volume of a standard 0.1 N NaCl aqueous solution to achieve a final volume of 25 mL with pH in the range from 1.0 to 12.0 (pH_0). After 48 h under magnetic stirring the pH of the resulting solutions was recorded (pH_{0f}). The same procedure of

mixture preparation at different pH_0 was repeated but with the addition of 0.1 g of composite and after 48 h of equilibration the pH was measured (pH_f). Data of $\Delta pH = (pH_f - pH_{0f})$ were calculated and plotted as a function of pH_{0f}.

Mathematical model

In this work, the RB5 dye adsorption mechanism onto the studied composite was described by a general three-resistance model [21] that includes dye transport on the film surrounding the composite particles, dye diffusion in the pores of the composite, and dye adsorption on the surface of the particles. The composite consists of an α-cellulose core, where only diffusion occurs, and a thin shell of magnetite nanoparticles immersed into a PPy matrix, where diffusion and adsorption occur. The equations describing the mathematical model were described elsewhere [16] with the difference that the Langmuir isotherm was used (they are also shown in the supplementary electronic information of this work). The equations of the mathematical model along with the initial and boundary conditions were simultaneously solved by the method of lines [22]. The radial coordinate was discretized using second-order finite differences [23]. Integration in time of discretized equations was performed using the stiff integrator ODE23s from Matlab®. Batch dye uptake data were used to estimate adsorption isotherm parameters. The forward rate coefficient, k_1, was estimated by fitting experimental dye batch uptake data along with the dye effective diffusivity using fminsearch from Matlab®. Both effective diffusivities, D_o and D_i, were considered as being equal for the sake of model simplicity.

3. Results and Discussion

Material characterization

Cellulose is a natural polymer that represents about one-third of plant tissues where it can be restocked by photosynthesis. Cellulose is ordered in micro-fibrils enclosed by hemicellulose and lignin [24]. The molecular structure of cellulose gives some advantages including low density, low extraction cost, recyclability, and biodegradablility [25]. Also due to the presence of the high donor reactivity of the hydroxyl group, which shows tendency to form intra- and inter-molecular hydrogen bonds; a broad chemical variability is present. These characteristics render cellulose as a potential material for composites

manufacturing [16]. Figure 2 shows the FTIR spectra of α-cellulose, magnetite nanoparticles, PPy, and the α-cellulose/magnetite/PPy composite. It can be seen that the characteristic signals corresponding to cellulose and PPy are present. Signals assignments of these two materials to the corresponding chemical group are summarized in Table 1. It can also be observed that the spectrum for the composite is similar to that corresponding to α-cellulose, with the main difference of the signal at 1562 cm^{-1}; which is related to a mixed C=C and inter-ring C-C vibrations of polypyrrole units. The peak at 1458 cm^{-1} derives from C–C polypyrrole ring stretching (Ovando-Medina et al. 2014). It is also observed that the cellulose signals corresponding to O-H and C-H stretching (3300 and 2900 cm^{-1}) are less intense in the composite, which is due to the presence of PPy coating cellulose fibers. Chemical bonding between cellulose fibers and PPy is desirable since cellulose would be more difficult to separate from the PPy layer. It would be expected that this bonding would take place through -OH groups of cellulose and the -NH groups of polypyrrole rings. From Figure 2, it can be observed that bands at 1551 and 1454 cm^{-1} for pure polypyrrole (inset in Figure 2) are shifted to 1562 and 1458 cm^{-1} for the composite. The observed shift of these bands may be due to chemical bonding between NH- in the pyrrole ring and the -OH groups of cellulose [26, 27]. FTIR signals corresponding to magnetite are usually observed between 500 and 600 cm^{-1}, therefore XRD analyses were performed to magnetite and the composite.

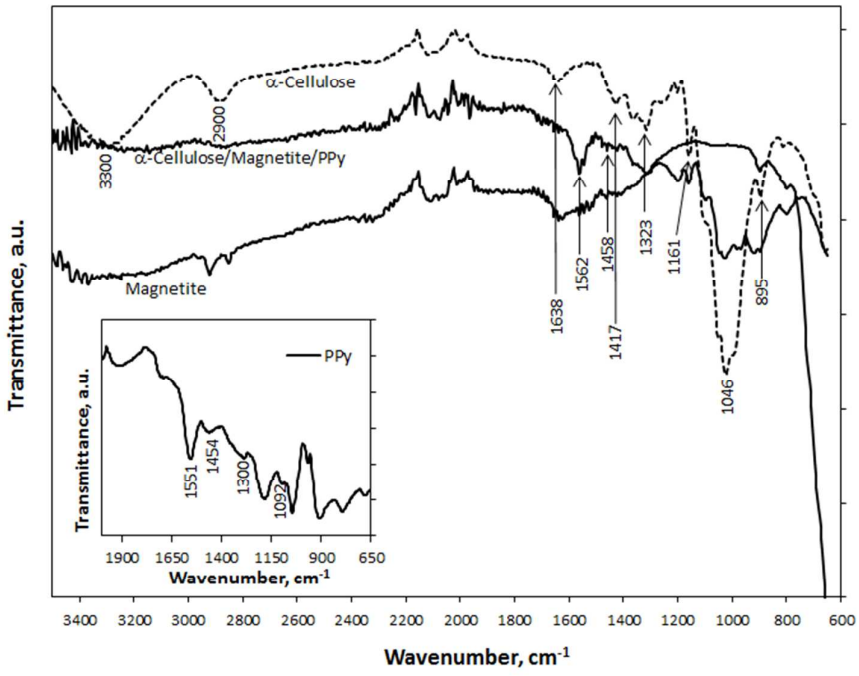

Fig. 2 FTIR spectra of α-cellulose, magnetite, PPy (inset), and the prepared composite

Figure 3a and 3b show the X-ray diffractograms of magnetite alone and the α-cellulose/magnetite/PPy composite. The positions of the diffraction peaks associated with the cubic crystal structures of Fe_3O_4 (magnetite) from the 190629 PDF card are shown as well. As can be seen (Figure 3a) the main peaks presented in the diffractograms are due to diffraction from the (220), (311), (222), (400), (422), (511), (440), (531), (620), and (533) planes; which are supposed to represent the typical Fe_3O_4 structure. The X-ray diffraction analysis corroborates that the sample is composed of Fe_3O_4 since there is a complete correspondence between the diffraction peaks and the database positions. The observed (strong and sharp) diffraction peaks suggest that the layers are highly crystalline. On the other hand the diffractogram corresponding to the composite (Figure 3b) only shows three broad peaks, which are due to the amorphous structure of PPy coating the cellulose and magnetite nanoparticles. In the XRD analysis only one peak is usually observed for PPy; depending on the synthesis process this peak is observed between 22° and 25° of 2θ [28]. In our case, the other signals can be due to the crystalline part of cellulose (15°, 22.5°, and 35° of 2θ) [29]; the XRD peaks corresponding to magnetite nanoparticles in the composite are almost imperceptible given the PPy coating.

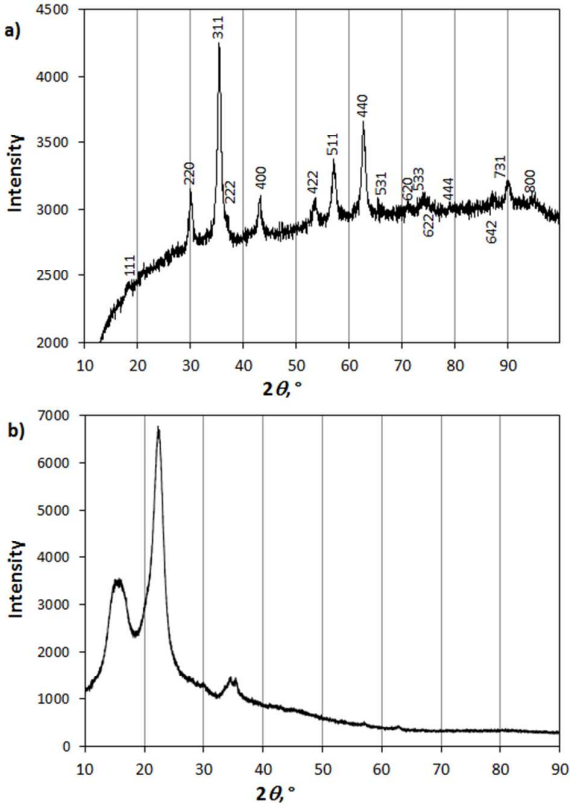

Fig. 3 XRD patterns for magnetite (a) and the α-cellulose/magnetite/PPy nanocomposite (b)

Thermogravimetric analysis was carried out to investigate the thermal properties of the α-cellulose/magnetite/PPy composite; the results are shown in Figure 4. As can be seen in this figure, magnetite nanoparticles are highly stable due to their inorganic nature; only 4% of weight loss was observed. α-cellulose showed a decomposition temperature around 260°C, nonetheless in the composite the onset of decomposition decreased to 200°C; which corresponds to PPy degradation. The decomposition rate was slower for the composite, which can be ascribed to the presence of magnetite nanoparticles that reduce PPy and α-cellulose chains mobility. In addition, the weight loss of composite after 550°C was 88.7% (11.3% of inorganic materials composed of magnetite nanoparticles and ashes from cellulose and PPy) whereas for α-cellulose the weight loss was close to 96.5% (3.5% of ashes); this implies that the composite contains 7.8% of magnetite nanoparticles even though 20% of magnetite was used in the preparation. We have calculated from PPy conversion and this magnetite amount that approximately 23% of PPy and magnetite are coating the α-cellulose fibers.

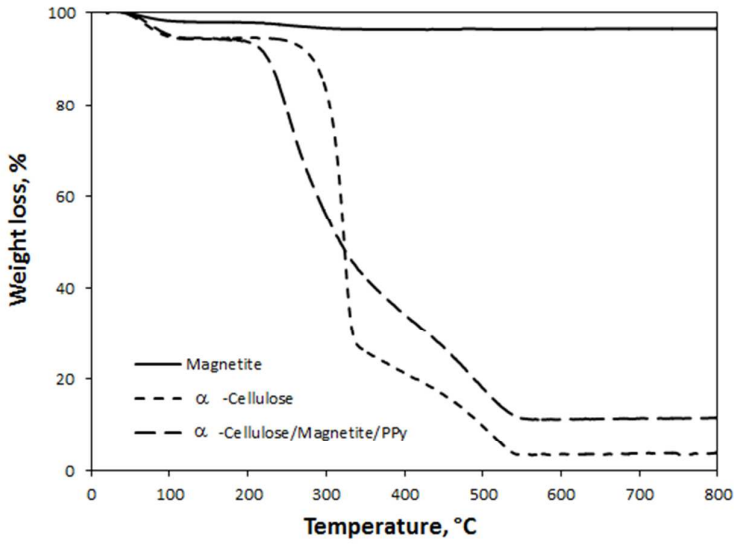

Fig. 4 TGA analyses of composite, magnetite nanoparticles, and α-cellulose

Figure 5 shows SEM images of uncoated α-cellulose (a), magnetite nanoparticles (b) and the α-cellulose/magnetite/PPy composite at two different magnifications (c and d). It can be observed that uncoated cellulose shows the typical surface of fibers reported in the literature with relatively homogeneous morphology compared to that observed for the as prepared composite (5c). Magnetite nanoparticles presented irregular morphology with small sizes ranging between 7 and 18 nm (Figure 5b). Figure 6 shows the particle size distribution of the synthesized magnetite nanoparticles. It can be observed that narrow PSD was obtained

through this process with a number-average particle size (Dn) of 13 nm and polydispersity index in size of 1.1; demonstrating the monomodal PSD shape. Sizes here observed are relatively small taking into account that the synthesis was made without any surfactant or template and are similar to those observed by Mascolo et al. [30] using different bases for magnetite precipitation. For example Goya et al. [31] reported magnetite nanoparticles sizes in the range from 5 to 150 nm when precipitating hematite particles by forced hydrolysis of a $FeCl_3$ solution at 100 °C for 2 days and further reduction under 1 atm of hydrogen at 360 °C for 3.5 h. Sun and Zeng [32] prepared magnetite nanoparticles by high-temperature solution-phase reaction of Fe(III) acetylacetonate in phenyl ether with alcohol, oleic acid, and oleylamine; obtaining sizes between 20 and 30 nm. From Figure 5c, it can be seen that the α-cellulose fibers and magnetite nanoparticles are coated by PPy, showing some PPy agglomerates. PPy consisted of well-defined monodispersed spherical particles (Figure 5d) with average diameter of 70 nm providing a large available surface area for chemical and physical interactions and electronic conductions. This PPy diameter is smaller than the observed value of 90 nm for PPy over pure α-cellulose previously reported [16], which demonstrates that magnetite nanoparticles affected the PPy nanoparticles size. The PPy morphology was typical of pyrrole polymerization on hydrophilic surfaces [33, 34].

Figure 7a shows a SEM image of the composite with contrast where two different materials can be observed; therefore EDS analyses were performed to the different zones marked with arrows in Figure 7a (Zones A and B). Figure 7b and 7c are the corresponding EDS spectra of these two zones. It can be seen that high C and O intensities are present in Figure 7b and a small amount of sulfur from traces of the APS used in pyrrole polymerization. Almost nothing of Fe was detected in zone A. EDS spectrum of zone B shows high concentrations of Fe and O (7c). Thus, we can conclude that the small brilliant zones in the composite (Figure 7a) mainly correspond to uncoated agglomerates of magnetite nanoparticles. Compositions in weight % and atomic % from the EDS analysis are shown in Table 2. From atomic percentages of Fe and O in this Table, we can calculate an O/Fe atomic ratio of 1.60; this value is 20% higher than the 1.33 expected for Fe_3O_4. The difference can be due to oxygen from -OH groups of the cellulose and the inherent analysis error.

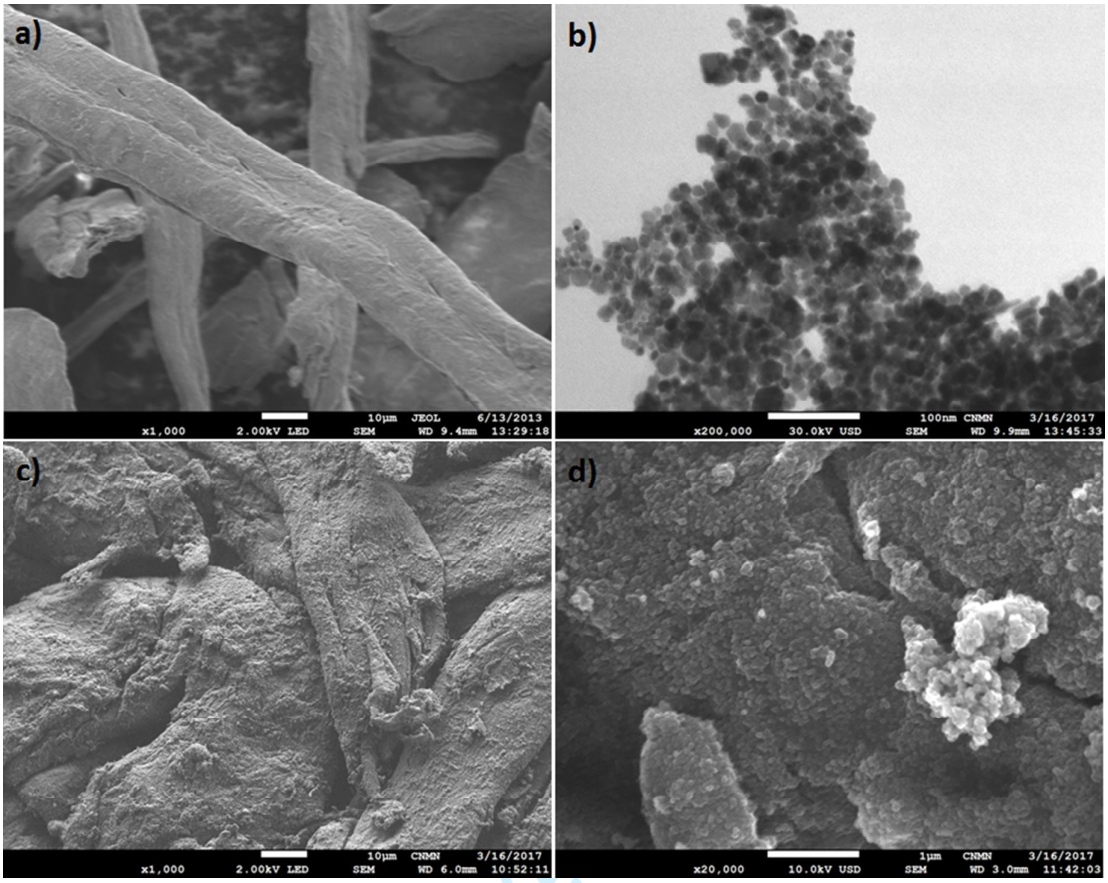

Fig. 5 SEM images of α-cellulose (a), synthesized magnetite nanoparticles in STEM mode (b), and SEM of the composite of α-cellulose/magnetite/PPy ×1000 (c) and ×20000 (d)

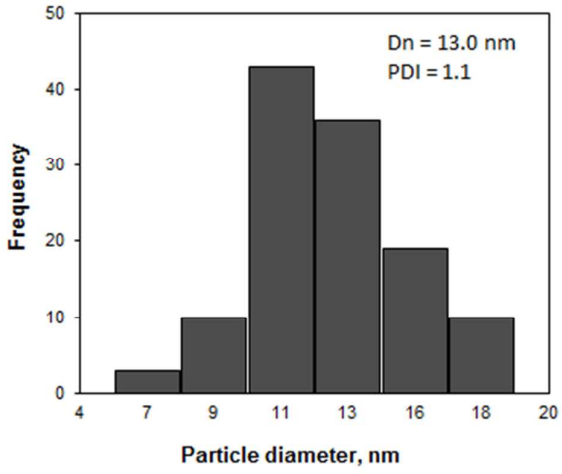

Fig. 6 PSD of magnetite nanoparticles

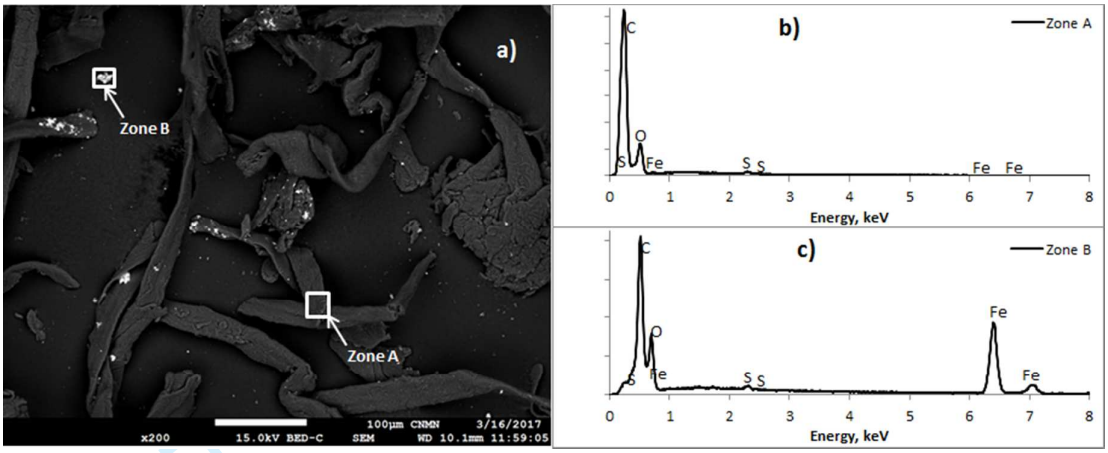

Fig. 7 SEM image of the composite with contrast (a), EDS spectra of zones A (b) and B (c)

Kinetics and batch adsorption experiments

The surface adsorption properties and the affinity between adsorbate and the adsorbent are described by the equilibrium adsorption isotherm. Equilibrium is reached when the concentration of sorbate in the solution is in dynamic balance with the concentration of the sorbate at the adsorbent interface. In this work, the experimental data of adsorption capacity in aqueous solutions were fitted by the Langmuir and Freundlich models:

Langmuir model:

$$Q_e = Q_m C_e/(1/K_L + C_e) \quad (1)$$

Freundlich model:

$$Q_e = K_F(C_e)^n \quad (2)$$

where Q_e is the adsorption capacity at the equilibrium concentration C_e, K_L is a Langmuir constant (related to the affinity of binding sites), Q_m is the maximum adsorption capacity, K_F is the Freundlich constant, and n is the surface heterogeneity constant in the Freundlich model.

The constants for these isotherms were evaluated by a least-squares method based on an optimization algorithm. The average absolute deviation percentage was calculated as follows:

$$\%D = \left(\frac{1}{N}\sum_{i=1}^{N}\left|\frac{Q_{exp}-Q_{pred}}{Q_{exp}}\right|\right) x\ 100\% \quad (3)$$

where N represents the number of data, Q_{exp} is the experimental adsorption capacity, and Q_{pred} is the predicted adsorption capacity. The Freundlich and Langmuir parameters corresponding to adsorption

experiments onto the α-cellulose/magnetite/PPy composite at different pH values are presented in Table 3. As can be seen from this table, the Langmuir model fits best the experimental data.

Figure 8a shows the adsorption isotherms (based on the total mass of composite) of the RB5 dye onto the α-cellulose/magnetite/PPy composite at pH 3.0, 4.0, and 7.0. It can be seen from Table 3 and Figure 8a that the maximum adsorption capacity decreases with the pH value of the dye solution. In other words, the dye adsorption energy at acidic pH is lower than that needed at a higher pH. This behavior can be explained with the point of zero charge (PZC) of the composite that is shown in Figure 8b. The PZC was determined as 1.2, this implies that in an aqueous dispersion of the composite with pH set to 1.2; the sum of + and – charges is zero at the surface of the composite. At higher pH values the surface is predominantly negative in character. It is noticeable that the composite showed an almost neutral charge in the pH interval from 1.2 to 3.2; if the pH value increases beyond 3.2 the surface charge becomes highly negative until a limit is reached at pH close to 9.0. The RB5 dye is an anionic molecule upon water dissociation as shown in Figure 1; therefore favorable electrostatic interactions between the dye and the surface of composite at pH below 3.2 are expected, where the zero point charge is almost reached. However, it is well known that other physical adsorption mechanisms can occur.

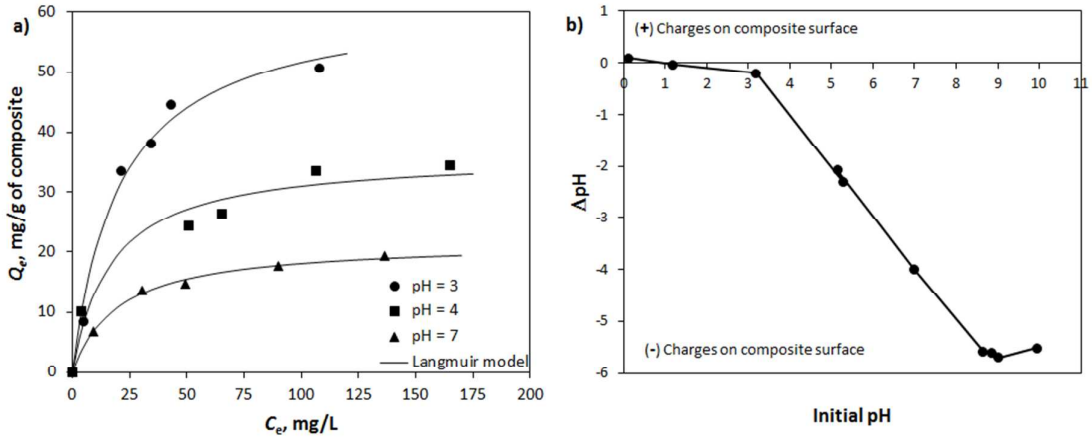

Fig. 8 (a) Isotherms of RB5 dye adsorption onto α-cellulose/magnetite/PPy composite at different pH values. (b) Point of zero charge curve for the synthesized composite

Figure 9 shows different proposed adsorption mechanisms of the RB5 dye onto the PPy nanoparticles coating cellulose and magnetite in the composite. The attachment through π–π* (bonding-antibonding) interactions between the electrons of the aromatic rings of the dye molecules and the electrons from pyrrole rings is

considered. High affinity of the dye for the composite surface can also result from hydrogen bond formation, which can be created between nitrogen from the pyrrole ring and nitrogen from the -NH_2 group of the dye as well as oxygen of uncoated magnetite with the -NH_2 group of the dye. Moreover, interactions between the oxygen atom from magnetite and the oxygen atom from hydroxyl groups or the nitrogen atom from the azo group of the dye through water molecules can exist. In order to differentiate electrostatic interactions from the others, we determined the active sites number through a titration method obtaining values of 1.97 meq/g of composite for the acid sites and 0.39 meq/g of composite for the basic sites. The maximum adsorption reached at pH = 3.0 was 62.31 mg/g of composite, which corresponds to 0.25 meq/g of composite. This value is 7.8 times smaller than the one determined for the acid active sites, which implies that not all the sites are available for adsorption; however, it is difficult to exactly discriminate the adsorption mechanisms. It is important to say that composite was recovered from the aqueous solutions using an external magnet; contributing to the simple application of the composite.

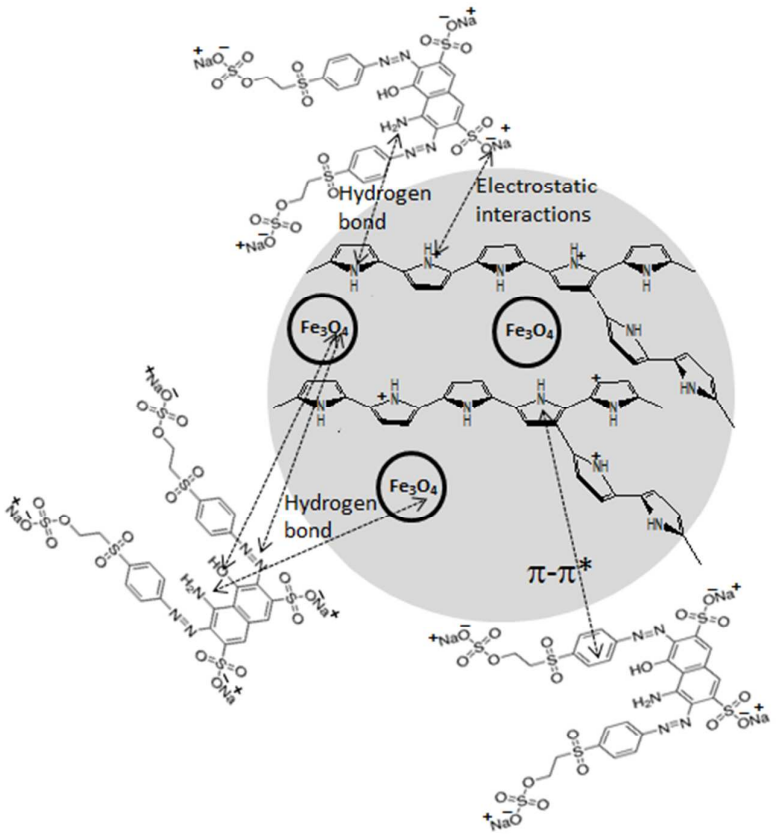

Fig. 9 Proposed interactions between the RB5 dye and the PPy coating from the studied composite (Modified from Wawrzkiewicz and Hubicki [35])

Figure 10a shows the hysteresis curve obtained from the N_2 adsorption-desorption analysis. It can be seen that the adsorbed N_2 amount was very low at any value of relative pressure. The hysteresis phenomenon can be associated with the capillary condensation in mesoporous structures. Different forms of the hysteresis loop are caused by different types of adsorbent and sorption environments (as temperature and pressure) [36]. According to IUPAC, the curve shown in Figure 10a corresponds to H3 hysteresis loop type and no micropores were observed since there is no tendency to form a plateau at low relative pressures [37]. The BET area (A_{BET}) of the composite was very low (11.42 m^2/g), which can be ascribed to deposition of PPy nanoparticles coating cellulose pores with pores of the resulting composite mainly due to PPy interparticle and intercluster spaces (Figure 10b).

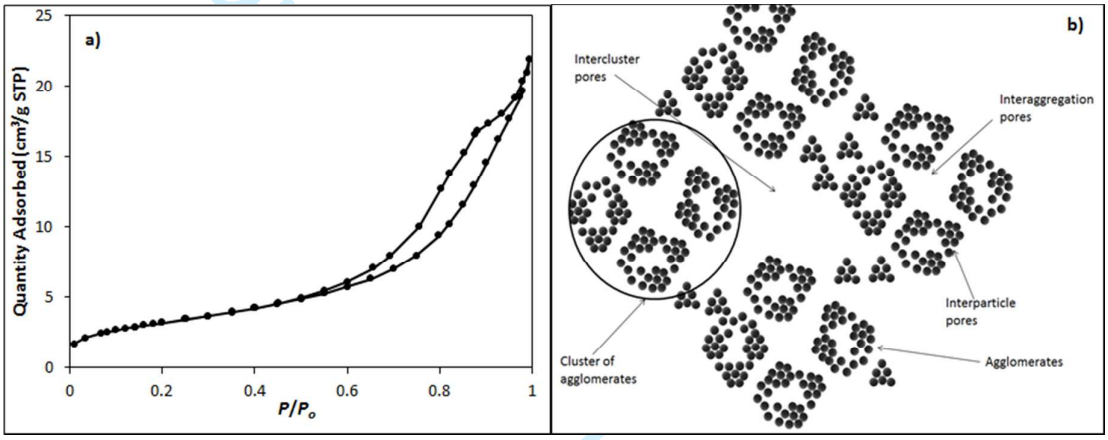

Fig. 10 (a) Hysteresis curve of N_2 adsorption-desorption for the synthesized composite and (b) proposed structural elements and pore types of PPy nanoparticles coating cellulose and magnetite in the composite

The experimental and simulated adsorption kinetics data for the RB5 dye at a pH value set to 3.0 using 0.1 g of composite and 100 mg/L of initial dye concentration are shown in Figure 11. The forward rate coefficient, k_1, was estimated by fitting the three-resistance mathematical model to the experimental dye batch uptake data along with the dye effective diffusivity using an initial dye concentration of 100 mg/L. Then, these optimized parameters were used to simulate the data for two conditions sets shown below. Table S1 of supplementary electronic information shows the values for all the non-fitted parameters used in the simulations. The value used for the apparent density (ρ_p) of the adsorbent particles was taken as 1.46 g/mL since cellulose density values are in the range from 1.3 to 1.5 g/mL [26]. Shell density (ρ_o) was fixed to 1.45 g/mL. Core porosity for cellulose powder (ε_i) was reported by Bhimte and Tayade [38] while shell porosity

for PPy and magnetite film (ε_o) was fixed to 0.35. From Figure 11, it can be seen that the mathematical model shows a good representation of the experimental adsorption kinetic data. The estimated values for k_1 and D_o where 7.30×10^{-7} L/mg·s and 4.37×10^{-11} m^2/s, respectively.

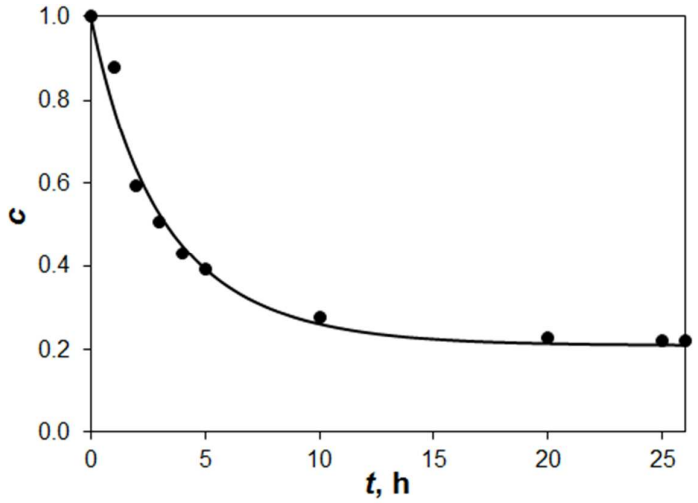

Fig. 11 Kinetics adsorption of the RB5 dye (dimensionless dye concentrations in the bulk liquid, c) at initial dye concentration C_A = 100 mg/L and using 0.1 g of composite

It is difficult to compare the adsorption rate coefficient with information in the literature since most of the times simplified models are used to describe adsorption of dyes [39-41] such as the pseudo-first order and the pseudo-second order models. Furthermore, these models are sensitive to the initial concentration of dye and multiple fittings need to be performed; moreover, these models are based on the dye concentration on the adsorbent discarding important resistances to mass transfer. To assess the predictive capacity of the mathematical model, two predictions were run. For the first run the mass of composite (W_A) and the initial dye concentration (C_A) were set to 0.15 g and 100 mg/L while for the second run C_A and W_A were set to 50 mg/L and 0.1 g, respectively. Figure 12 shows both predictions along with the experimental results of batch uptake experiments. It can be seen that the mathematical model performs a fair prediction of the batch dye adsorption behavior using the studied composite.

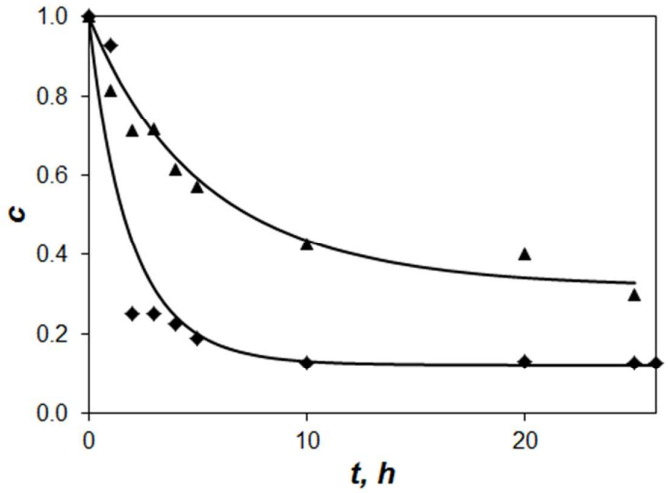

Fig. 12 Kinetics adsorption of RB5 dye (dimensionless dye concentrations in the bulk liquid, *c*) at initial dye concentration C_A = 50 mg/L and 0.1 g of composite (triangles); and C_A = 100 mg/L and 0.15 g of composite (diamonds)

4. Conclusions

A composite of α-cellulose/magnetite nanoparticles/PPy was prepared and characterized. It was observed that magnetite presented the typical cubic crystal structure corresponding to Fe_3O_4, and irregular morphology with average size of 13.0 nm and monomodal PSD. Also, the composite consisted of PPy nanoparticles with approximate size of 70 nm coating α-cellulose fibers and magnetite nanoparticles. This composite showed a low BET area (11.42 m^2/g), which was ascribed to the presence of mosopores derived from interparticle and intercluster spaces of PPy particles. The composite showed potential as adsorbent of the RB5 dye from aqueous solutions at acidic pH, the adsorption derived from electrostatic interactions between the dye and the positively charged surface of the composite at this pH value. The adsorption process was defined by the Langmuir isotherm with a maximum adsorption capacity of 62.31 mg of RB5 dye/g of composite. Kinetics of RB5 dye adsorption was well described with the three-resistance mathematical model obtaining, for the experiments set to initial pH of 3.0, a D_o of 4.37×10^{-11} m^2/s and k_1 of 7.30×10^{-7} L/mg·s.

Acknowledgements

Camerina J. Guzmán Álvarez acknowledges a scholarship from CONACYT for MSc studies through the Grant PDCPN-2015-384, #25941.

Author Contributions: Víctor M. Ovando-Medina and Paola E. Díaz-Flores conceived the idea, designed the experiments and wrote the paper; Camerina J. Guzmán-Álvarez performed the experiments and discussed part of the results; Hugo Martínez-Gutiérrez performed the SEM analysis; Omar González-Ortega implemented and discussed the mathematical model.

Conflict of interest: authors declare no conflict of interest

References

1. The United Nations World Water Development Report 2017 (2017). Wastewater: The Untapped Resource. *The United Nations World Water Development Report*, Paris. http://unesdoc.unesco.org/images/0024/002475/247552e.pdf. Accessed 21 July 2017.
2. Water and wastewater International: case study: textile dyeing without effluent. http://www.waterworld.com/articles/wwi/2017/02/case-study-textile-dyeing-without-effluent.html (2017). Accessed 02 August 2017.
3. B.H. Hameed, D.K. Mahmoud, A.L. Ahmad, Equilibrium modeling and kinetic studies on the adsorption of basic dye by a low-cost adsorbent: Coconut (Cocos nucifera) bunch waste, J. Hazard. Mater., 158 (2008) 65–72.
4. I.A.W. Tan, A.L. Ahmad, B.H. Hameed, Adsorption of basic dye on high-surface-area activated carbon prepared from coconut husk: Equilibrium, kinetic and thermodynamic studies, J. Hazard. Mater., 154 (2008) 337–346.
5. B. Noroozi, G.A. Sorial, H. Bahrami, M. Arami, Equilibrium and kinetic adsorption study of a cationic dye by a natural adsorbent—Silkworm pupa, J. Hazard. Mater., 139 (2007) 167–174.
6. K.Y. Hor, J.M.C. Chee, M.N. Chong, B. Jin, C. Saint, P.E. Poh, R. Aryal, Evaluation of physicochemical methods in enhancing the adsorption performance of natural zeolite as low-cost adsorbent of methylene blue dye from wastewater, J. Clean. Prod. 118 (2016) 197–209.
7. O.A. Saputra, M.D. Prameswari, V.T.D. Kinanti, O.D. Mayasari, Y.D. Sutarni, K. Apriany, W.W. Lestari, Preparation, characterization and methylene blue dye adsorption ability of acid activated-natural zeolite, OP Conf. Ser.: Mater. Sci. Eng., (2017) https://doi.org/10.1088/1757-899X/172/1/012039

8. I. Humelnicu, A. Băiceanu, M.-E. Ignat, V. Dulman, The removal of Basic Blue 41 textile dye from aqueous solution by adsorption onto natural zeolitic tuff: Kinetics and thermodynamics, Process. Saf. Environ. Prot., 105 (2017) 274–287.
9. R. Aziam, M. Chiban, E. Eddaoudi, A. Soudani, M. Zerbet, F. Sinan, Factors controlling the adsorption of acid blue 113 dye from aqueous solution by dried C. edulis plant as natural adsorbent, Arab. J. Geosci., (2016) https://doi.org/10.1007/s12517-016-2675-4
10. A. Pérez-Escobedo, P.E. Díaz-Flores, J.R. Rangel-Méndez, F.J. Cerino-Cordova, V.M. Ovando-Medina, J.A. Alcalá-Jáuregui, Fluoride adsorption capacity of composites based on chitosan-zeolite-algae, Rev. Mex. Ing. Quím., 15 (2016) 139–147.
11. U. Habiba, T.A. Siddique, T.C. Joo, A. Salleh, B.C. Ang, A.M. Afifi, Synthesis of chitosan/polyvinyl alcohol/zeolite composite for removal of methyl orange, Congo red and chromium(VI) by flocculation/adsorption, Carbohyd. Polym., 157 (2017) 1568–1576.
12. H. Wang, T. Lin, A. Kaynak, Polypyrrole nanoparticles and dye absorption properties, Synth. Met. 151 (2005) 136–140.
13. V.M. Ovando-Medina, P.E. Díaz-Flores PE, H. Martínez-Gutiérrez, L.A. Moreno-Ruiz, Antonio-I.D. Carmona, M. Hernández-Ordoñez, Composite of cellulosic agricultural waste coated with semiconducting polypyrrole as potential dye remover, Polym. Compos., 35 (2014) 186–193.
14. M. Banimahd-Keivani, K. Zare, H. Aghaie, R. Ansari, Removal of methylene blue dye by application of polyaniline nano composite from aqueous solutions, J. Phys. Theor. Chem. IAU Iran, 6 (2009) 63–70.
15. R. Ansari, Z. Mosayebzadeh, Removal of basic dye methylene blue from aqueous solutions using sawdust and sawdust coated with polypyrrole, J. Iran. Chem. Soc., 7 (2010) 33–35.
16. V.M. Ovando-Medina, J. Vizcaíno-Mercado, O. González-Ortega, J.A. Rodríguez de la Garza, H. Martínez-Gutiérrez, Synthesis of α-cellulose/polypyrrole composite for the removal of reactive red dye from aqueous solution: Kinetics and equilibrium modeling, Polym. Compos. 36 (2015) 312–321.
17. A.R. Bagheri, M. Ghaedi, A. Asfaram, A.A. Bazrafshan, R. Jannesar, Comparative study on ultrasonic assisted adsorption of dyes from single system onto Fe_3O_4 magnetite nanoparticles loaded on activated carbon: Experimental design methodology, Ultrason. Sonochem., 34 (2017) 294–304.

18. L. Bai, Z. Li, Y. Zhang, T. Wang, R. Lu, W. Zhou, H. Gao, S. Zhang, Synthesis of water-dispersible graphene-modified magnetic polypyrrole nanocomposite and its ability to efficiently adsorb methylene blue from aqueous solution, Chem. Eng. J., 279 (2015) 757–766.
19. M. Ayad, N. Salahuddin, A. Fayed, B.P. Bastakoti, N. Suzuki, Y. Yamauchi, Chemical design of a smart chitosan–polypyrrole–magnetite nanocomposite toward efficient water treatment, Phys. Chem. Chem. Phys., 16 (2014) 21812-21819.
20. A.A. Asgharinezhad, H. Ebrahimzadeh, Coextraction of acidic, basic and amphiprotic pollutants using multiwalled carbon nanotubes/magnetite nanoparticles@polypyrrole composite, J. Chromatogr. A, 1412 (2015) 1–11.
21. R.M. Montesinos, R. Guzmán, A. Tejeda-Mansir, Simulation of stirred tank affinity processes applied to separation of proteins, Int. J. Bio-Chromatogr., 6 (2001) 231–243.
22. S. Chapra, R. Canale, Numerical methods for engineers, McGraw-Hill, New York, 1983.
23. C.J. Geankoplis, Transport processes and unit operations, Allyn and Bacon, Boston, 1983.
24. J.I, Morán, V.A. Alvarez, V.P. Cyras, A. Vázquez, Extraction of cellulose and preparation of nanocellulose from sisal fibers, Cellulose, 15 (2008) 149–159.
25. X. Li, L.G. Tabil, S. Panigrahi, Chemical treatments of natural fiber for use in natural fiber-reinforced composites: A review, J. Polym. Environ., 15 (2007) 25–33.
26. J.H. Johnston, F.M. Kelly, J. Moraes, T. Borrmann, D. Flynn, Conducting polymer composites with cellulose and protein fibres, Curr. Appl. Phys., 6 (2006) 587–590.
27. D. Müller, C.R. Rambo, D.O.S. Recouvreux, L.M. Porto, G.M.O. Barra, Chemical in situ polymerization of polypyrrole on bacterial cellulose nanofibers, Synth. Met. 161 (2011) 106–111.
28. N. Su, H.B. Li, S.J Yuan, S.P. Yi, E.Q. Yin, Synthesis and characterization of polypyrrole doped with anionic spherical polyelectrolyte brushes, Express Polym. Lett. 6 (2012) 697–705.
29. A. Kumar, Y.S. Negi, V. Choudhary, N.K. Bhardwaj, Characterization of cellulose nanocrystals produced by acid-hydrolysis from sugarcane bagasse as agro-waste, J. Mat. Phys. Chem., 2 (2014) 1–8.
30. M.C. Mascolo, Y. Pei, T.A. Ring, Room temperature co-precipitation synthesis of magnetite nanoparticles in a large pH window with different bases, Materials, 6 (2013) 5549–5567.

31. G.F. Goya, T.S. Berquó, F.C. Fonseca, Static and dynamic magnetic properties of spherical magnetite nanoparticles, J. Appl. Phys., 94 (2003) 3520–3528.
32. S. Sun, H. Zeng, Size-controlled synthesis of magnetite nanoparticles, J. Am. Chem. Soc. 124 (2002) 8204–8205.
33. J.H. Johnston, J. Moraes, T. Borrmann, Conducting polymers on paper fibres, Synth. Met. 153 (2005) 65–68.
34. G. Nyström, A. Mihranyan, A. Razaq, T. Lindström, L. Nyholm, M. Strømme, A Nanocellulose polypyrrole composite based on microfibrillated cellulose from wood, J. Phys. Chem. B, 114 (2010) 4178–4182.
35. M. Wawrzkiewicz, Z. Hubicki, In: A. Kilislioglu, Ion Exchange - Studies and Applications, InTech, pp. 37–72.
36. L. Qi, X. Tang, Z. Wang, X. Peng, Pore characterization of different types of coal from coal and gas outburst disaster sites using low temperature nitrogen adsorption approach, Int. J. Mining Sci. Tech., 27 (2017) 371–377.
37. L.F. Ballesteros, J.A. Teixeira, S.I. Mussatto, Chemical, functional, and structural properties of spent coffee grounds and coffee silverskin, Food Bioprocess Tech., 7 (2014) 3493–3503.
38. N.A. Bhimte, P.T. Tayade, Evaluation of microcrystalline cellulose prepared from sisal fibers as a tablet excipient: a technical note. AAPS Pharm. Sci. Tech. 8 (2007) E56–E62.
39. Z. Eren, F.N. Acar, Adsorption of reactive black 5 from an aqueous solution: equilibrium and kinetic studies, Desalination ,194 (2006) 1–10.
40. T.K. Saha, N.C. Bhoumik, S. Karmaker, M.G. Ahmed, H. Ichikawa, Y. Fukumori, Adsorption characteristics of reactive black 5 from aqueous solution onto chitosan, CLEAN–Soil, Air, Water, 39 (2011) 984–993.
41. D. Karadag, M. Turan, E. Akgul, S. Tok, A. Faki, Adsorption equilibrium and kinetics of reactive black 5 and reactive red 239 in aqueous solution onto surfactant-modified zeolite, J. Chem. Eng. Data, 52 (2007) 1615–1620.

Table 1. FTIR assignments of the main signals of PPy and cellulose.

IR signals corresponding to PPy	
Signal, cm^{-1}	**Chemical group**
1551	C=C backbone stretching
1454	C–C ring stretching
1300	C–H in-plane
1092	C–N stretching vibrations
Main signals corresponding to cellulose	
895	stretching COC at b-glycosidic linkage.
1046	stretching CO at C6
1161	stretching COC at b-glycosidic linkage
1323	bending CH_2 (wagging) at C–6
1417	bending CH_2 (sym) at C–6
1638	-O- tensile vibration neighboring hydrogen atoms
2900	stretching C-H
3300	stretching O-H (hydrogen bonded)

Table 2. Compositions in weight and atomic percentages determined from EDS analyses of zones A and B shown in Figure 7a.

Element	**Zone A**			**Zone B**		
	Weight %	Atomic %	Error %	Weight %	Atomic %	Error %
C $_K$	69.63	75.52	4.04	---	---	---
O $_K$	29.8	24.26	9.51	31.41	61.52	5.12
S $_K$	0.45	0.18	7.16	---	---	---
Fe $_K$	0.12	0.03	58.26	68.59	38.48	2.86

Table 3. Estimated parameters of Langmuir and Freundlich models calculated from experimental equilibrium batch adsorption data at different pH.

Langmuir model				
pH	Q_m	K_L	R^2	**%D**
3	62.31	0.048	0.96	11.8
4	36.19	0.059	0.88	13.2
7	21.67	0.050	0.98	2.20
Freundlich model				
pH	K_F	n	R^2	**%D**
3	9.35	0.379	0.81	28.1
4	6.87	0.324	0.97	3.50
7	4.04	0.324	0.93	7.50

* Q_m in mg/g; K_L in $mg^{-1}L^{-1}$; K_F in $mg^{1-n}L^{n}g^{-1}$

Electronic supplementary information of paper:

Synthesis of α-cellulose/magnetite/polypyrrole composite for the removal of reactive black 5 dye from aqueous solutions

Víctor M. Ovando-Medina, Camerina J. Guzmán-Álvarez, Paola E. Díaz-Flores, Hugo Martínez-Gutiérrez, Omar González-Ortega

Dye uptake model

In this work, the reactive black 5 dye batch adsorption kinetics using the proposed composite is presented. A mathematical model was used to fit the experimental data to determine the values of selected parameters. The model is a general three-resistance model that includes the transport on the film that surrounds the composite particles, diffusion inside the particles and adsorption on the surface of the particles. The proposed composite is visualized as a core-shell particle with cellulose as core and magnetite-containing polypyrrol as shell. The studied dye is allowed to diffuse in both the core and the shell while adsorption only occurs on the shell.

The batch adsorption process consists of a bulk liquid and a solid (composite). Since the bulk liquid is considered well-stirred such that a macroscopic balance on the dye can be performed, this results in Eq. 1 where the movement of dye in the boundary layer produces a temporal change in dye concentration in the liquid outside the composite

$$V_L \frac{dC}{dt} = -3\frac{W_A k_f}{\rho_p R_o}\left(C - C_o\big|_{R=R_o}\right) \tag{1}$$

Where V_L is the liquid volume (mL), W_A is the adsorbent weight (g), ρ_p is the apparent density of the adsorbent particle (g/mL), k_f is the boundary layer mass transfer coefficient (m/s), R_o is the external composite radius (m), C is the dye concentration in the bulk liquid (mg/L), C_o is the dye concentration in the liquid within the adsorbent shell (mg/L), t is the time coordinate (s), and R in the radial coordinate (m).
In the composite shell a microscopic balance on the dye in the liquid results in Eq. 2. This balance considers temporal and radial variations of the dye concentration in the liquid within the shell, along with a dye transfer from the liquid to the surface of the shell.

$$\varepsilon_o \frac{\partial C_o}{\partial t} + \rho_o \frac{\partial Q_o}{\partial t} = D_o\left(\frac{\partial^2 C_o}{dR^2} + \frac{2}{R}\frac{\partial C_o}{\partial R}\right) \qquad R_i \le R \le R_o \tag{2}$$

Where ε_o is the shell porosity, ρ_o is the shell density (g/mL), D_o is the effective diffusivity of the dye in the shell (m^2/s), R_i is the composite core radius (m), and Q_o is the dye concentration on the surface of the adsorbent (mg/g of shell).
A microscopic balance on the dye in the liquid results in Eq. 3. It is similar to Eq. 2 but with no possibility of adsorption.

$$\varepsilon_i \frac{\partial C_i}{\partial t} = D_i\left(\frac{\partial^2 C_i}{dR^2} + \frac{2}{R}\frac{\partial C_i}{\partial R}\right) \qquad 0 \le R \le R_i \tag{3}$$

Where ε_i is the core porosity, D_i is the effective diffusivity in the core (m^2/s), and C_i is the dye concentration in the liquid inside the adsorbent core.

Eq. 2 requires a constitutive equation to describe the adsorption process in terms C_o and Q_o. In this work a second order forward reaction (adsorption) and a first order backward (desorption) reaction were considered (Eq. 4). At equilibrium, Eq. 4 reduces to the Langmuir isotherm (Eq. 5).

$$\frac{\partial Q_o}{\partial t} = k_1 C_o\left(Q_m - Q_o\right) - k_2 Q_o \tag{4}$$

$$Q_{oe} = \frac{Q_m C_{oe}}{K_d + C_{oe}} \tag{5}$$

Where k_1 is the forward rate constant (L/mg·s), k_2 is the backward rate constant (1/s), K_d (k_2/k_1) is the equilibrium desorption constant (mg/L), Q_m is the maximum adsorption capacity for the shell (mg/g), C_{oe} is the dye concentration in the liquid within the adsorbent shell at equilibrium (mg/L), and Q_{oe} is the dye concentration in the surface of the adsorbent shell at equilibrium (mg/g).
The initial conditions for Eq. 1-4 are reported in Eq. 6-9. At the beginning, the dye molecules only exist in the bulk liquid.

$$C = C_A \tag{6}$$

$$C_i = 0, \qquad 0 \le R \le R_i \tag{7}$$

$$C_o = 0, \qquad R_i \le R \le R_o \tag{8}$$

$$Q_o = 0, \qquad R_i \le R \le R_o \tag{9}$$

where C_A is the initial dye concentration in the bulk liquid (mg/L). A no-flux condition at the center of the composite particles establishes the boundary condition given by Eq. 10.

$$R = 0, \qquad \frac{\partial C_i}{\partial R} = 0, \qquad t > 0 \tag{10}$$

A surface mass balance on the dye at the core/shell interface of the composite results in Eq. 11 (second boundary condition). It establishes the continuity of the diffusion process when the dye molecules leave the shell and enter the core.

$$R = R_i, \qquad D_o \frac{\partial C_o}{\partial R} = D_i \frac{\partial C_i}{\partial R}, \qquad t > 0 \tag{11}$$

To complete the dye adsorption model, another surface mass balance on the dye at the surface of the composite results in Eq. 12. Similar to Eq. 1, it establishes the continuity of the convective flux (dye molecules crossing the boundary layer) with the diffusive flux (dye molecules entering the liquid inside the shell).

$$R = R_o, \qquad k_f\left(C - C_o\right) = D_o \frac{\partial C_o}{\partial R}, \qquad t > 0 \tag{12}$$

The mathematical model (Eq. 1-12) was set dimensionless by using the variables presented in Eq. 13-16. Eq. 13 defines dimensionless dye concentrations in the bulk liquid, pores of the shell, and pores of the core. Eq. 14 defined dimensionless adsorbed dye concentration while Eq. 15 defines a dimensionless radial position. Finally, Eq. 16 defines the dimensionless temporal coordinate.

$$c = \frac{C}{C_A}, \qquad c_i = \frac{C_i}{C_A}, \qquad c_o = \frac{C_o}{C_A} \tag{13}$$

$$q_o = \frac{Q_o}{Q_m} \tag{14}$$

$$r = \frac{R}{R_o} \tag{15}$$

$$\tau = \frac{D_o t}{\varepsilon_o r_o^2} \tag{16}$$

The resulting dimensionless mathematical model is

$$\frac{dc}{d\tau} = -3N \left.\frac{\partial c_o}{\partial r}\right|_{r=1} \tag{17}$$

$$\frac{\partial c_o}{\partial \tau} + \xi \frac{\partial q_o}{\partial \tau} = \left(\frac{\partial^2 c_o}{dr^2} + \frac{2}{r}\frac{\partial c_o}{\partial r}\right) \qquad r_i \le r \le r_o \tag{18}$$

$$\frac{\partial c_i}{\partial \tau} = D\left(\frac{\partial^2 c_i}{dr^2} + \frac{2}{r}\frac{\partial c_i}{\partial r}\right) \qquad 0 \le r \le r_i \tag{19}$$

$$\frac{\partial q_o}{\partial \tau} = \phi^2\left[\lambda c_o\left(1 - q_o\right) - q_o\right] \tag{20}$$

With initial conditions

$$c = 1 \tag{21}$$

$$c_i = 0, \qquad 0 \le r \le r_i \tag{22}$$

$$c_o = 0, \qquad r_i \le r \le r_o \tag{23}$$

$$q_o = 0, \qquad r_i \le r \le r_o \tag{24}$$

And boundary conditions

$$r = 0, \qquad \frac{\partial c_i}{\partial r} = 0, \qquad \tau > 0 \tag{25}$$

$$r = \frac{R_i}{R_o}, \qquad D_o \frac{\partial c_o}{\partial r} = D_i \frac{\partial c_i}{\partial r}, \qquad \tau > 0 \tag{26}$$

$$r = 1, \qquad \mathrm{Bi}(c - c_o) = \frac{\partial c_o}{\partial r}, \qquad \tau > 0 \tag{27}$$

Where the resulting dimensionless parameters are:

$$N = \frac{\varepsilon_o W_A}{V_L \rho_p}, \qquad \xi = \frac{\rho_o Q_m}{\varepsilon_o C_A}, \qquad D = \frac{\varepsilon_o D_o}{\varepsilon_i D_i}, \qquad \phi^2 = \frac{k_2 \varepsilon_o R_o^2}{D_o}, \qquad \lambda = \frac{C_A}{K_d}, \qquad \mathrm{Bi} = \frac{k_f R_o}{D_o} \tag{28}$$

Model solution and parameter estimation

The batch uptake kinetics mathematical model (Eq. 17-20) along with the initial and boundary conditions (Eq. 21-27) were solved using the method of lines. The dimensionless radial coordinate was discretized using second-order finite differences. Integration in dimensionless time of the resulting ordinary differential equations was performed using stiff integrator ODE23s from Matlab. Batch dye uptake experiments were conducted to estimate adsorption isotherm parameters Q_m and K_d. The film mass transfer coefficient was calculated using the correlation by Geankoplis (Eq. 29).

$$k_f = \frac{D_{AB}}{r_o} + 0.31 \left(\frac{\mu_L}{\rho_L D_{AB}} \right)^{-2/3} \left(\frac{\Delta \rho \mu_L g}{\rho_L^2} \right)^{1/3} \tag{29}$$

Where D_{AB} is the dye diffusivity (m^2/s), μ_L is the liquid viscosity (kg/m·s), ρ_L is the liquid viscosity (kg/m^3), $\Delta\rho$ is the density difference (ρ_p-ρ_L) between the composite particle and the liquid (kg/m^3), and g is gravity acceleration (m/s^2). Dye diffusivity was estimated using the Wilke-Chang method according to the empirical modification of the Stokes-Einstein relation (Eq. 30).

$$D_{AB} = \frac{7.4 \times 10^{-12} (\varphi M_B)^{1/2} T}{\eta_B V_A^{0.6}} \tag{30}$$

Where φ is the association factor of liquid (equal to 2.6 for water), M_B is the solvent molecular weight (g/mol), T is the temperature (K), V_A is the molar volume of dye at boiling temperature (cm^3/mol), and η_B is the solvent viscosity (cP). For the case of the

studied dye, its molar volume was estimated using the method of Schroeder presented in Eq. 31.

$$V_A = 7\left(N_C + N_H + N_O + N_N + N_{DB}\right) + 24.5N_{Cl} + 21N_S - 7 \quad (31)$$

Where N_C is the number of carbon atoms, N_H the number of hydrogen atoms, N_O the number of oxygen atoms, N_N the number of nitrogen atoms, N_{DB} the number of double bonds, N_{Cl} the number of chlorine atoms, and N_S the number of sulfur atoms.
The forward rate constant, k_1, was estimated by fitting experimental dye batch uptake data along with the dye effective diffusivity using fminsearch from Matlab. Both effective diffusivities, D_o and D_i, were considered as being equal for the sake of simplicity.

Table S1. Non-fitted parameters used in the mathematical model

Parameter	Value	Units
C_A	100	mg/L
V_L	30	mL
W_A	0.1	g
ρ_p	1.46	g/mL
ρ_o	1.45	g/mL
r_o	227.3×10^{-6}	m
r_i	212.5×10^{-6}	m
ε_o	0.35	
ε_i	0.28	
Q_m	260.7	mg/g shell
K_d	20.72	mg/L
N_C	26	
N_H	21	
N_N	5	
N_O	19	
N_{Cl}	0	
N_S	6	
N_{DB}	12	
V_A	700	cm^3/mol
φ	2.6	
M_B	18	g/mol
T	298.15	K
η_B	1	cP
D_{AB}	2.96×10^{-10}	m^2/s
μ_L	0.001	kg/m·s
ρ_L	1000	kg/m^3
g	9.81	m/s^2

k_f	2.41×10^{-5}	m/s